CHAPTER 1

LOAD FREQUENCY CONTROL IN A SINGLE AREA POWER SYSTEM.

1.1   INTRODUCTION

Power system is used for the conversion of natural energy to electric energy. For the optimization of electrical equipment, it is necessary to ensure the electric power quality. It is known three phase AC is used for transportation of electricity. During the transportation, both the active and reactive power balance must be maintained between the generation and utilization AC power. When either frequency or voltage changes equilibrium point will shift. Good quality of electrical power system means both the voltage and frequency to be fixed at desired values irrespective of change in loads that occurs randomly. It is in fact impossible to maintain both active and reactive power without control which would result in variation of voltage and frequency levels. To cancel the effect of load variation and to keep frequency and voltage level constant a control system is required. Though the active and reactive powers have a combined effect on the frequency and voltage, the control problem of the frequency and voltage can be separated. Frequency is mostly dependent on the active power and voltage is mostly dependent on the reactive power. Thus, the issue of controlling power systems can be separated into two independent problems. The active power and frequency control are called as load frequency control (LFC). The most important task of LFC is to maintain the frequency constant against the varying active power loads, which is also referred as un- known external disturbance.

Power exchange error is an important task of LFC. Generally, a power system is composed of several generating units. To improve the fault

tolerance of the whole power system, these generating units are connected through tie-lines. This use of tie-line power creates a new error in the control problem, which is the tie-line power exchange error. When sudden change in active power load occurs to an area, the area will get its energy through tie-lines from other areas. Eventually the area that is subject to the change in load should balance it without external support. Or else there will be economic conflicts between the areas. This is why each area requires separate load frequency controller to regulate the tie line power exchange error so that all the areas in an interconnected system can set their set points differently. In short, the LFC has two major duties, which are to maintain the desired value of frequency and also to keep the tie line power exchange under schedule in the presence of any load changes. Also, the LFC has to be unaffected by unknown external disturbances and system model and parameter variation.

1.1.1 REASONS FOR THE NEED OF MAINTAINING CONSTANTFREQUENCY:

- The speed of ac. motors are directly related to the frequency.

- If the normal operating frequency is 50 Hz and the turbines run at speeds corresponding to frequencies less than 47.5 Hz or above 52.5 Hz, then the blades of the turbines may get damaged.

- The operation of a transformer below the rated frequency is not desirable. When frequency goes below rated frequency at constant system voltage then the flux in the core increases and then the transformer core goes into the saturation region.

- Loads and other electrical equipment are usually designed to operate at a particular frequency. Off-nominal frequency operation causes electrical loads to deviate from the desired output. The output of power plant

4

auxiliaries like pumps or fans may reduce, causing reduction in power plant output.

1.1.2 LOAD FREQUENCY CONTROL:

If the system is connected to numerous loads in a power system, then the system frequency and speed change with the characteristics of the governor as the load changes. If it's not required to maintain the frequency constant in a system then the operator is not required to change the setting of the generator. But if constant frequency is required the operator can adjust the velocity of the turbine by changing the characteristics of the governor when required. If a change in load is taken care by two generating stations running parallel then the complex nature of the system increases. The ways of sharing the load by two machines are as follow:

1) Suppose there are two generating stations that are connected to each other by tie line. If the change in load is either at A or at B and the generation of A is regulated so as to have constant frequency then this kind of regulation is called as **Flat Frequency Regulation.**

2) The other way of sharing the load is that both A and B would regulate their generations to maintain the frequency constant. This is called **parallel frequency regulation.**

3) The third possibility is that the change in the frequency of a particular area is taken care of by the generator of that area thereby maintain the tie-line loading. This method is known as **flat tie- line loading control**.

4) In **Selective Frequency control** each system in a group is taken care of the

load changes on its own system and does not help the other systems, the group for changes outside its own limits.

5) In **Tie-line Load-bias control** all the power systems in the interconnection aid in regulating frequency regardless of where the frequency change originates.

1.2 MATHEMATICAL MODELLING OF A LFC SYSTEM:

1.2.1 MATHEMATICAL MODELLING OF AGENERATOR:

With the use of swing equation of a synchronous machine to small perturbation, we have

$$\frac{2H}{\omega}\frac{d^2\Delta\delta}{dt^2} = \Delta\text{Pm} - \Delta P_e \qquad (2.1)$$

Or in terms of small change in speed

$$\frac{d\Delta\frac{\omega}{\omega s}}{dt} = \frac{1}{2Hs}\big(\Delta\text{Pm(s)} - \Delta\text{P}_e(s)\big) \qquad (2.2)$$

Laplace Transformation gives,

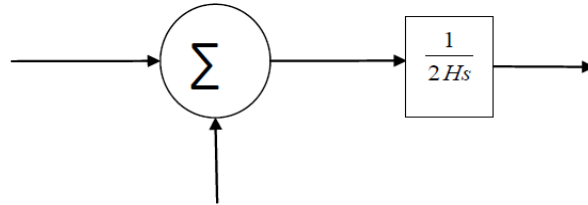$$\Delta\boldsymbol{\Omega(s)} = \frac{1}{2Hs}\big(\Delta\text{Pm(s)} - \Delta\text{P}_e(s)\big) \qquad (2.3)$$

Fig 2.1: Mathematical modelling block diagram for a generator.

1.2.2 MATHEMATICAL MODELLING OFLOAD:

The load on a power system consists of variety of electrical drives. The load

speed characteristic of the load is given by:

$$\Delta P_e = \Delta P_L + D \Delta\omega \qquad\qquad (2.4)$$

where ΔP_L is the non-frequency sensitive

change in load, $D\Delta\omega$ is the load change that is

frequency sensitive.

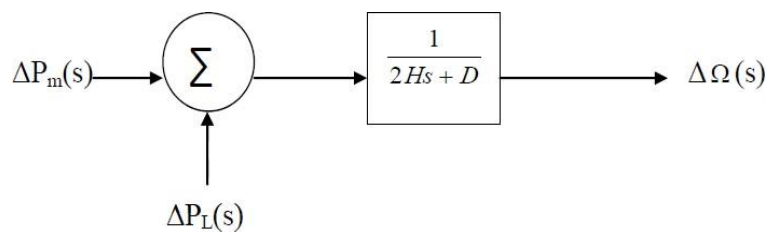D is expressed as percentage change in load divided by percentage change in frequency.

Fig 2.2: Mathematical modelling Block Diagram of Load.

1.2.3 MATHEMATICAL MODELLING FOR PRIMEMOVER:

The source of power generation is the prime mover. It can be hydraulic turbines near waterfalls, steam turbine whose energy come from burning of coal, gas and other fuels. The model of turbine relates the changes in mechanical power output ΔP_m and the changes in the

steam valve position ΔP_V.

$$G_T = \frac{\Delta P_m(s)}{\Delta P_V(s)} = \frac{1}{1+\tau s}. \qquad (2.5)$$

where the turbine constant is in the range of 0.2 -2.0.

1.2.4 MATHEMATICAL MODELLING FOR GOVERNOR:

When the electrical load is increased suddenly then the electrical power exceeds the input mechanical power. This deficiency of power in the load side is compensated from the kinetic energy of the turbine. Due to this reason the energy that is stored in the machine is decreased and the governor sends signal for supplying volumes of water, steam or gas to increase the speed of the prime mover to compensate deficiency in speed.

$$\Delta P_g = \Delta P_{ref} - \frac{1}{R}\Delta f. \qquad (2.6)$$

The command ΔPg is transformed through amplifier to the steam valve position command ΔPV. We assume here a linear relationship and considering simple time constant we get this s-domain relation.

$$\Delta P_v = \frac{1}{1+\tau s}\Delta P_g(s). \qquad\qquad (2.7)$$

Combining all the above block diagrams, for an isolated area system we get the following:
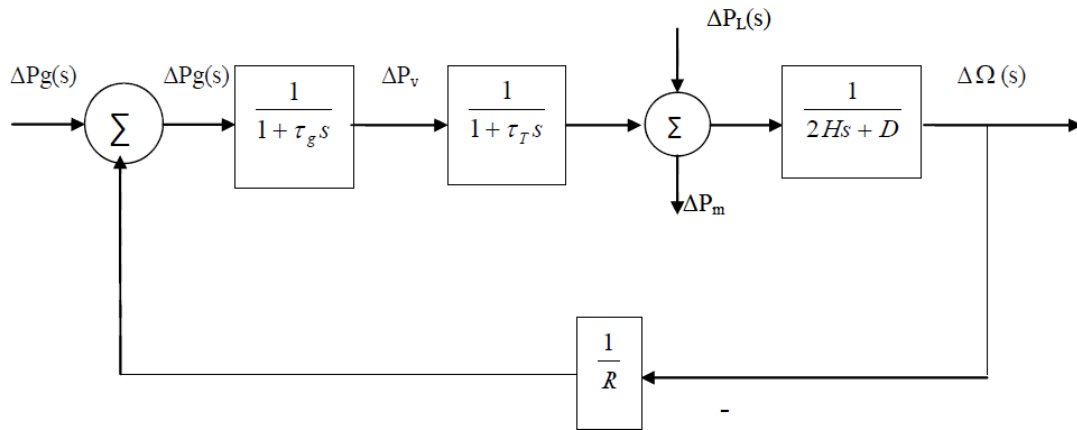

Fig 2.5: complete block diagram of single area system.

The closed loop transfer function that relates the load change ΔP_L to the frequency deviation $\Delta\Omega$ is

$$\frac{\Delta\Omega(s)}{-\Delta P_L} = \frac{(1+\tau_g s)(1+\tau_T s)}{(1+\tau_g s)(1+\tau_g s)(2Hs+D)+{}^1\!/_R} \qquad (2.8)$$

1.3 AUTOMATIC GENERATIONCONTROL:

If the load on the system is suddenly increased,

then the speed of the turbine drops before the governor could adjust the input of the steam to this new load. As the change in the value of speed decreases the error signal becomes lesser and the position of the governor and not of the fly balls gets nearer to the point required to keep the speed constant. One way to regain the speed or frequency to its actual value is to add an integrator on its way. The integrator will monitor the average error over a certain period of time and will overcome the offset. Thus, as the load in the system changes continuously the generation is adjusted automatically to restore the frequency to its nominal value. This method is known as automatic generation control. In an interconnected system consisting of several areas, the task of the AGC is to divide the load among the system, stations and generators so to achieve maximum economy and uniform frequency.

1.3.1 AGC IN A SINGLEAREA:

With the main LFC loop, change in the system load will result in a steady state frequency deviation, depending on the speed regulation of the governor. To reduce the frequency deviation to zero we need to provide a reset action by using an PI controller to act on the load reference setting to alter the speed set point. This PI controller would make changes that the final frequency deviation to become zero. The PI controller gain need to be adjusted for obtaining satisfactory transient response.

The closed loop transfer function of the control system is given by:

$$\frac{\Delta\Omega(\mathbf{s})}{-\Delta P_L} = \frac{(1+\tau_g s)(1+\tau_T s)}{(1+\tau_g s)(1+\tau_g s)(2Hs+D)+K_P K_I + \frac{1}{R}} \qquad (2.8)$$

1.4 FREQUENCY RESPONSES OF LFC SYSTEM:

An isolated power station has the following

parameters Turbine time constant = 0.5 s

Governor time constant = 0.2 s

Governor inertia constant = 5 s

Governor speed regulation = R

per unit

The load varies by 0.8 per cent for a 1 per cent change in frequency (D=0.8)

The governor speed regulation is set to R = 0.05 per unit. The turbine rated

output is 250 MW at nominal frequency 50 Hz. A sudden load change of 50

MW (ΔP_L= 0.2 Per unit) occurs.

Find steady state Frequency deviation in Hz. Also obtain time domain

performance specifications and the frequency deviation step response.

1.4.1 FREQUENCY RESPONSE WITHOUT THE PI CONTROLLER:

To obtain the time domain specifications and the step response following

command is used: Pl= 0.2; num= [0.1 0.7 1];

den= [1 7.08 10.56 20.8];

t= 0:.02:10;

c= -pl* step (num, den, t);

plot (t, c), xlabel ('t, sec'),

ylabel('pu');title ('Frequency deviation

step response');

grid timespec (num, den);
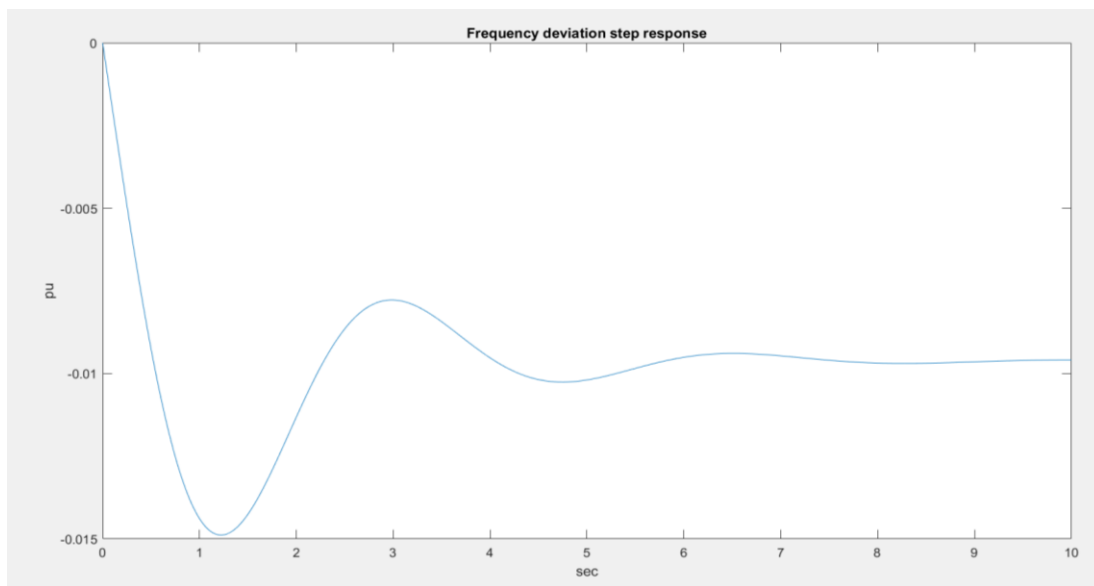

Fig 1.4.1Frequency deviation step response without using PI controller.

The time domain specifications are:

Peak time=1.223 Percentage overshoot=54.80

Rise time= 0.418

Settling time= 6.8

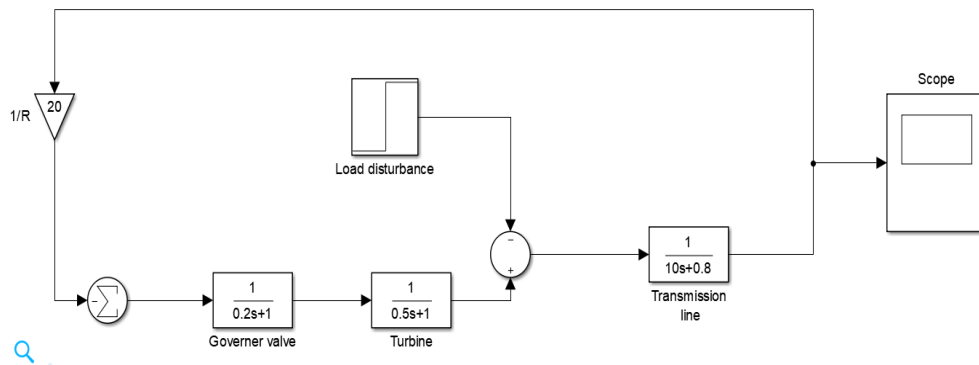 The Simulink model for the above system is:

Fig 1.4.2 Simulation Block Diagram of the system without using PI controller.

1.4.2 FREQUENCY RESPONSE WITH THE PI CONTROLLER:

Substituting the system parameters, we get the closed loop

transfer function as: T(s)= (0.1s3+ 0.7s2+ s)/ (s4+ 7.08s3+

10.56s2+ 20.8s+ 7)

To find the step response following command is used:

pl= 0.2;

ki= 7;

num= [0.1 0.7 1 0];

den= [1 7.08 10.56 20.8 7];

t= 0:.02:12;

c= -pl* step (num,

den, t); plot (t, c),

grid

xlabel ('t, sec'), ylabel('pu') title

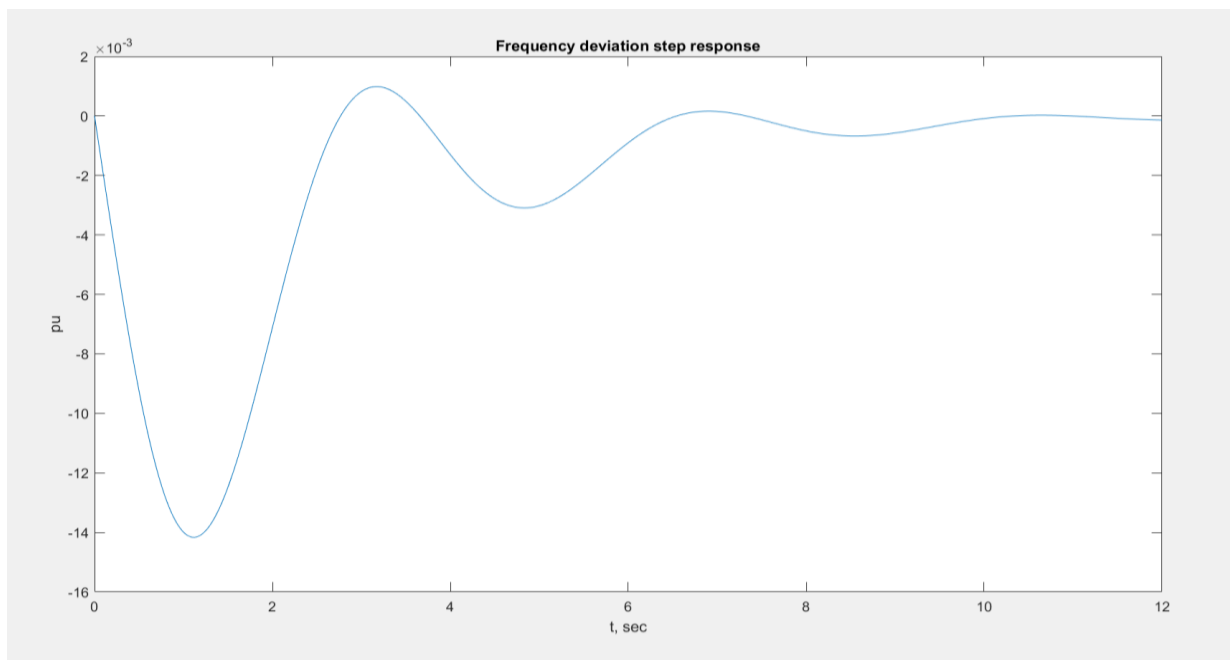('Frequency deviation step

response')

Fig 1.4.3 Frequency deviation step response with using PI controller.

From the step response we have seen that the steady state frequency deviation is zero, and the frequency returns to its actual value in approximately 10seconds.
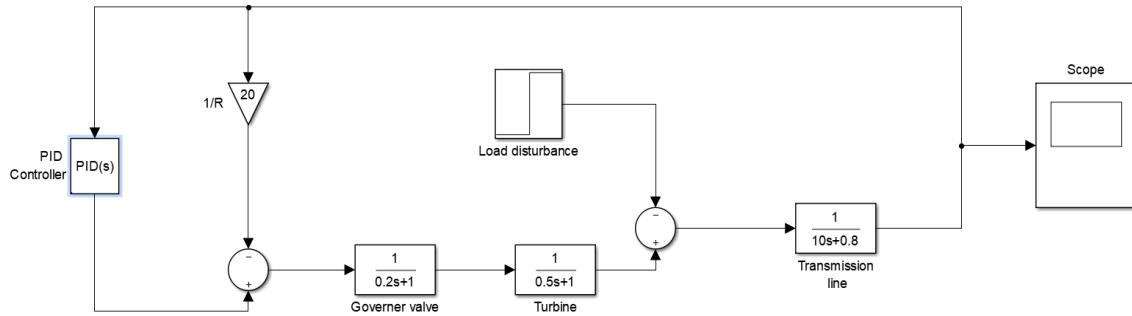
\
The Simulink model for the above system is:

Fig 1.4.4 Simulation Block Diagram of the system with using PI controller.

The above discussion shows the load frequency control of a single area power system. The MATLAB results gives the frequency responses of the load frequency control of a single area power system with proportional-integral controller and without proportional-integral controller. In the forthcoming chapters, the Electric Vehicle to Grid Technology integrated with Load frequency control systems and its mathematical modeling will be discussed.

1.5 CONCLUSION.
 The above discussion shows the load frequency control of a single area power system. The MATLAB results gives the frequency responses of the load frequency control of a single area power system with proportional-integral controller and without proportional-integral controller.

Chapter 2: Electric Vehicle to Grid Technology

2.1. INTRODUCTION:

In response to the need for the additional power source in emergency situations, it is expected that large fleets of electric vehicles (EVs) will constitute an important share of the electricity demand. This evolution is likely to be accompanied by a parallel evolution of the electricity supply with the deployment of smart grid technologies. As a consequence, it is expected that demand will feature higher potential for communication and control, which will enable its active participation in the daily operational planning of power systems. In particular, EVs being equipped with a battery can both defer their demand or inject electricity back into the system. However, to achieve volumes that can have an impact on the system, these demands need to be aggregated and operated as an ensemble. This permits the scheduling of EV charging and services in coordination with the system operator thus enhancing the power system's efficiency and security while reducing its environmental impact.

2.2. CONCEPT OF ELECTRIC VEHICLE TO GRID TECHNOLOGY:

The vehicle-to-grid (V2G) concept aims to optimize the way we transport, use and produce electricity by turning electric cars into 'virtual power plants'. Under this relatively new concept, electric cars would store and dispatch <u>electrical energy stored</u> in networked vehicle batteries which together act as one collective battery fleet for 'peak shaving' (sending power back to the grid when demand is high) and 'valley filling' (charging at when needed).

V2G would allow consumers to charge electric vehicles and monitor their energy costs, using mobile devices. This information helps utilities to better manage grid loads during peak times. The information on the car's state of charge, the vehicle location and the type of power source are managed by the Electric Vehicle Aggregator. Collected data is sent to the PI controller, depending on the grid load, power is extracted from Electric Vehicle.

When the electric utility would like to buy power from the V2G network, it holds an auction. The car owners or leasing companies would be able to define the parameters under which they will sell energy from their battery pack.

BALANCING TO GRID

There are peak times and off-peak times for energy use, just like there's rush hour traffic in the morning and in the evening.

Balancing the grid is about making sure there's enough electricity on the network when we need it in peak times, so the country doesn't black out. And it also stops power surges, which could damage domestic appliances, or cause electrical fires.

As mentioned earlier, more renewable energy sources are being used to create electricity for the grid. This is a key part of the nation's move towards a zero carbon future, and a cleaner, greener country for us all. But it makes balancing the grid more tricky – as solar and wind can't be produced on demand in the same way as fossil fuel energy can.

With technology like EV smart charging, it is far more in control when the vehicle is charging. And with V2G, the vehicle owner can also make money from feeding energy back into the grid, to "balance" it in times of need.

2.3.0 Electric Vehicle:

EVs can be roughly divided into two big classes PEVs (plug-in EVs) and non-plug-in EVs, which are essentially HEVs (hybrid EVs). **Plug-in electric vehicles (PEVs)** use electricity from the energy grid to charge large battery packs, then use the batteries to power an electric motor. In addition, PEVs can be further split into PHEVs (plug-in hybrid EVs) and BEVs (battery EVs). While BEVs are characterized by the use of batteries to supply their electric propulsion system, PHEVs are generally equipped with smaller batteries because they employ an internal combustion engine; this can directly propel the vehicle and/or recharge the battery on board, resulting in an extended mobility range compared to BEVs. EVs could be utilized in a wide range of applications such as smoothing of renewable energy sources and frequency regulation using vehicle-to-grid techniques. Fast power output of EV batteries and thereby the fast response characteristic provides the opportunity to introduce Electric Vehicle to Grid Technology. EVs can be used as generators or loads and hence reduce generation/demand fluctuations, and improve frequency response. For practical participation of EVs in frequency regulation market, a new entity called as EVs aggregator is required to aggregate and control large number of EVs in order to satisfy the frequency regulation criteria. EVs could be effectively used for not only frequency regulation but also for improving stability of smart grid systems

when inevitable communication time delays are observed. Furthermore, the dynamic model of an EV battery system is usually first-order transfer function as follows:

$$G_{EV} = \frac{\Delta P_{EV}}{U_C(s)} = \frac{K_{EV}}{1 + sT_{EV}}$$

where, K_{EV} and T_{EV} represent gain and time constant of the EVs battery system, respectively. The turbine of the generator from Generation station and the EVs aggregator have participation ratios of α_0 and α_1 which are allocated to determine their participation in frequency regulation service. For example, $\alpha_1 = 1$ means that the turbine is totally employed to regulate the system frequency. Note that the total amount of α_0 and α_1 is equal to one and is also total contribution of both generation units (Grid and Electric Vehicle) for frequency regulation service.

2.4.0 Why do we use Plug in Electric vehicle for V2G technology?

Since they are usually powered by batteries that can store it is easier to deliver energy to the grid when needed. This way, PEVs can work as a distributed generators and provide different services when they are parked and connected to an electrical outlet. Exploiting these services add an extra economic value to PEVs, making them more profitable for PEV owners and accelerating their market. Also, due to the fact that PEV batteries charging period at rated power generally requires much less time than plug-in parking periods, it is possible to optimize the PEV charging process from the economical point of view . However, PEV batteries can also be employed to reduce negative impacts of PEVs on power systems, even increasing their performances.

2.5.0 What is V2G charging or EV smart charging?

V2G charging refers to the 2-way flow of electrical energy from the grid, through a specially-built charger into an EV, and back again. As an EV owner, one can choose to charge the car up from the grid – or sell stored energy in the car back to the grid.

2.6.0 Electric Vehicle Aggregator:

The massive deployment of the EV and interaction with the power system (i.e., transmission and distribution system operators) requires an agent responsible for aggregating EV and managing their charging process. This agent is called aggregator and it is an enabler of the EV integration in the electricity market and power system operations. *In other words,* Electric vehicles aggregator is an intermediate between electric vehicle (EV) and operator of power grid. The EVs aggregator is responsible for the management of EVs in order to supply the owners with their orders and also for maximizing the profits of power grid in electricity market.

The main function of EV aggregator is to send and receive information regarding the charging status of EV's in order to adjust their power using an automatic generation control in V2G technology.

2.6.1 AN EV AGGREGATOR MODEL:

An EV aggregator model consisting of a large number of EVs, each of which has a delay component. The dynamic model of an EV battery system is usually described as the following first-order transfer function:

$$G_{EV} = \frac{\Delta P_{EV}}{U_C(s)} = \frac{K_{EV}}{1 + sT_{EV}}$$

where K_{EV} denotes the gain of the EV and T_{EV} denotes the time constant of the EV battery system. The delay taken for receiving control signals from the EV aggregator is modeled as an exponential transfer function of $e^{-s\tau(t)}$, where $\tau(t)$ denotes a time-varying delay function which models the communication delay from the EV aggregator to the EV and the scheduling delay in the EV aggregator.

For analytical simplicity, we assume that the delays for all EVs are the same as T_{delay} on an average sense and the time constants T_{EV} of all EVs are the same. From the assumption, we obtain an aggregated EV aggregator model consisting of one delay function and one EV dynamics model.
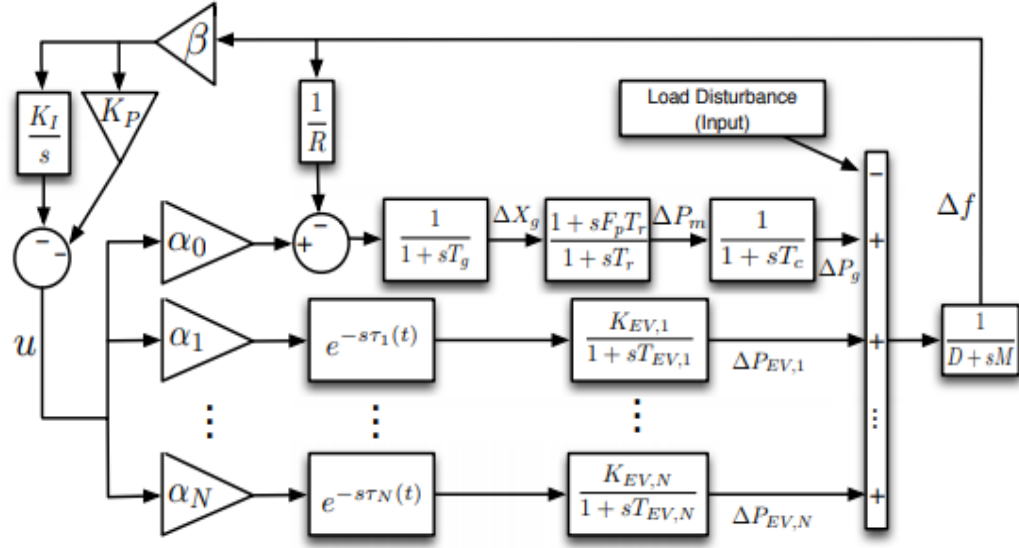
Fig.2.1: LFC system integrated with an EV aggregator.

2.6.2 LFC Model including EV Aggregators with Delays:

Fig. 1 shows a single-area LFC model including multiple EV aggregators with time-varying delays. Except the model of EV aggregators with time-varying delays, other components have been modeled in many LFC-related studies. We assume that all synchronous generators have reheat thermal turbines. We adopt, as an LFC controller, a PI-type controller which has been used for LFC in Germany, Netherlands, Belgium, etc. The output of the PI controller is distributed to the reheat thermal generator and N EV aggregators depending on the participation ratios α_0, α_1,....,α_N, where α_0 denotes the participation ratio of an aggregated thermal generator and α_i denotes the participation ratio of EV aggregator i for i = 1......N.

The linearized dynamic model of the single-area LFC model including *N* EV aggregators with time-varying delays can be expressed as follows:

$$x(t) = Ax(t) + B_0 u(t) + \sum_{k=1}^{N} B_k u(t - \tau_k(t)) + F\Delta P_d$$
$$y(t) = Cx(t)$$

(2.1)

Where

$$x(t) = [\Delta f \ \Delta P_g \Delta P_m \Delta X_g \Delta P_{EV,1} \ ... \ \Delta P_{EV,N}]^T$$
$$y(t) = ACE,$$
$$B_0 = [0 \ 0 \ 0 \ \frac{F_p \alpha_0}{T_g} \frac{\alpha_0}{T_g} \ 0 \ \cdots \ 0 \ ]^T$$

$$B_k = \frac{\alpha_k K_{EV,K}}{T_{EV,K}} e_{4+k}, \quad (k = 1, \ldots, N)$$

$$C = [\,\beta\ 0\ 0\ 0\ 0 \cdots 0\,],$$

$$F = \left[\,-\frac{1}{M}\ 0\ 0\ 0\ 0\ \cdots\ 0\right]^T$$

$$A = \begin{bmatrix} \dfrac{-D}{M} & \dfrac{1}{M} & 0 & 0 & \dfrac{1}{M} & \cdots & \dfrac{1}{M} \\[2ex] 0 & \dfrac{-1}{T_c} & \dfrac{1}{T_c} & 0 & 0 & \cdots & 0 \\[2ex] \dfrac{-F_p}{RT_g} & 0 & \dfrac{-1}{T_r} & \dfrac{T_g - F_p T_r}{T_r T_g} & 0 & \cdots & 0 \\[2ex] \dfrac{-1}{RT_g} & 0 & 0 & \dfrac{-1}{T_g} & 0 & \cdots & 0 \\[2ex] 0 & 0 & 0 & 0 & \dfrac{-1}{T_{EV,1}} & \cdots & 0 \\[2ex] \vdots & \vdots & \vdots & \ddots & \ddots & \cdots & \vdots \\[2ex] 0 & 0 & 0 & 0 & 0 & \cdots & \dfrac{-1}{T_{EV,N}} \end{bmatrix}$$

And

$\Delta f, \Delta X_g, \Delta P_m$ and ΔP_g denote the derivation of the frequency, valve position, mechanical power output and generator power output, respectively. $\Delta P_{EV,1}$ (k=1,....N) is the derivation of the power output in the k-th EV aggregator.

The ACE signal is defined as follows:

$$ACE = \beta \Delta f.$$

A PI-type LFC controller is designed as follows:

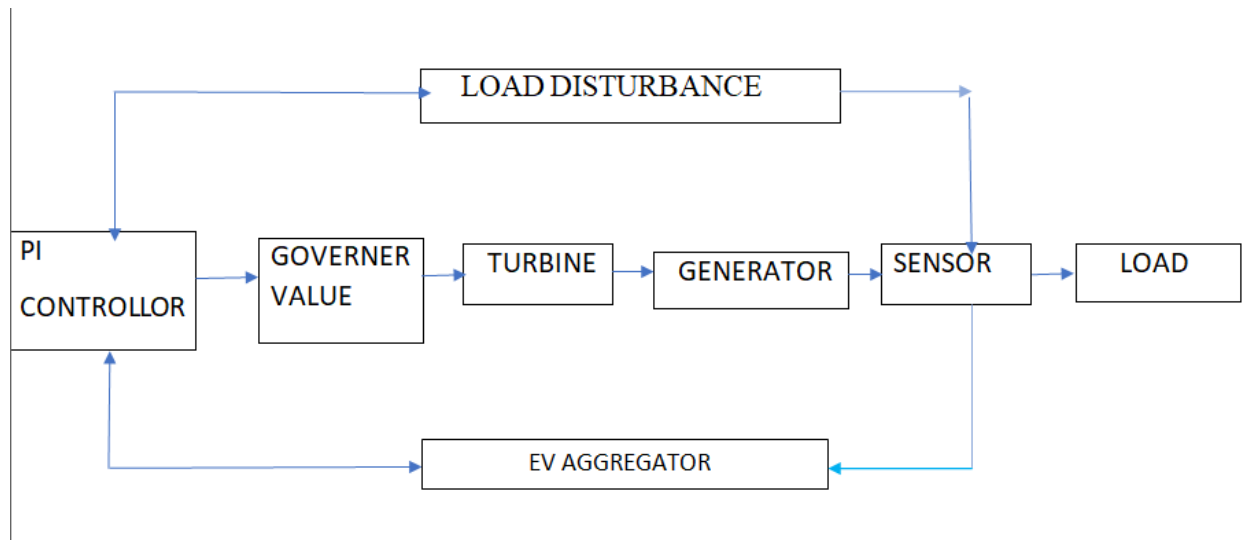$$u(t) = -K_p ACE - K_I \int ACE \, dt. \tag{2.2}$$

Fig 2.2 Electric Vehicle to Grid Technology

Fig.2.2 shows the block diagram of Electric vehicle to grid technology. The load disturbance is sensed using frequency sensor. Whenever there is heavy power demand, the frequency of voltage of the tie lines connecting the consumer and the grid reduces. This is reduction in frequency is sensed by frequency sensor. The load disturbance sensed by frequency sensor is feedback to Proportional-Integral Controller. The PI controller in turn decides how much power to be extracted from EV aggregator along with the Gird to compensate the power requirements. According to PI controller's instruction, the governor valve is opened to let the necessary amount of steam to generate more power. The turbine takes input(steam) from governor and does its work. The generator in turn takes the output of turbine as its input and converts into electrical energy. Meanwhile, the amount of power to be extracted from EV aggregator also comes into picture. The power generated from the Grid and the power extracted from the EV aggregator is now distributed to load.

In this chapter, Electric vehicle to grid technology and EV aggregator model are discussed. In next chapter mathematical modeling of Load Frequency Control System integrated with EV aggregator will be discussed.

CHAPTER-3
MATHEMATICAL MODELLING OF LOAD FREQUENCY CONTROL SYSTEMS INTEGRATED WITH EV AGGREGATOR

3.1.0 INTRODUCTION:

The design and implementation of load frequency control systems integrated with Electric Vehicle Aggregator need to be supported by a holistic understanding of their functional processes, their interactions, and their responses to various changes. Models developed to represent different functional processes and the systems are seen as useful tools to support the related studies for different stakeholders in a tangible way. This chapter presents an overview of modeling approaches applied to support aggregation of EVs with Load Frequency Control System. As already known, in the integrated electrical systems, frequency control service considering the Electric Vehicle (EV) aggregators could lead to time variable delay in Load Frequency Control Schemes. Thus, this chapter illustrates different time-variable delays result based on the stability of an LFC system in the presence of the EV aggregators. Primarily, a graphical method characterizing the stability boundary locus is implemented. For a given time delay, the method computes all the stabilizing proportional-integral (PI) controller gains, which constitutes a stability region in the parameter space of PI controller. Secondly, in order to complement the stability regions a frequency-domain exact method is used to calculate stability delay margins for various values of PI controller gains. The impact of EV aggregator on both stability regions and stability delay margins is thoroughly analyzed and the results are authenticated by the usage of visual programming (MATLAB) and time domain simulation.

3.1.1 MATHEMATICAL MODELLING OF LFC SYSTEM WITH EV AGGREGATOR:

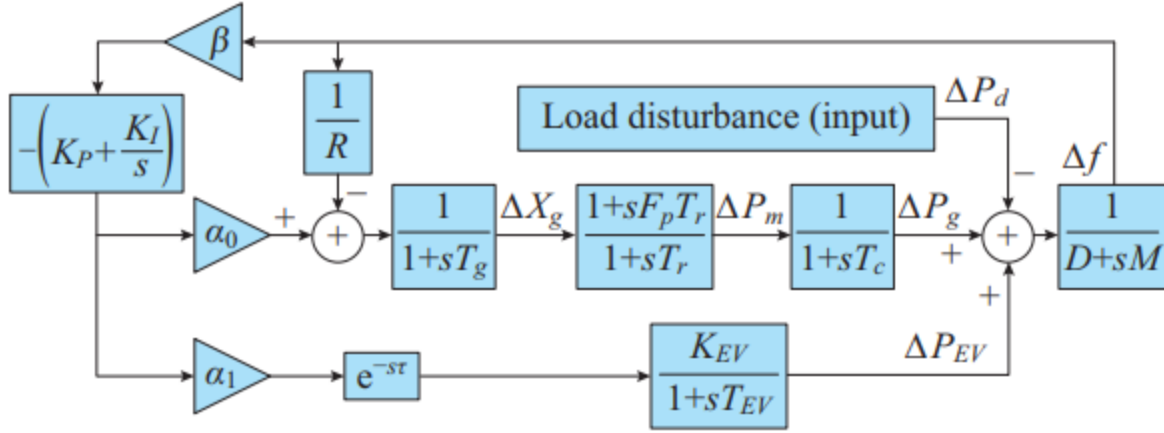The block diagram of a single area LFC system including an EV aggregator and delay block is presented in Fig.1

Fig 3.1   System model of single-area LFC with EV aggregator.

The PI type controller is adopted as LFC controller. In Fig.1, $\Delta f, \Delta X_g, \Delta P_m$, ΔP_{EV} and ΔP_d are the deviation of frequency, valve position, mechanical power output, generator power output, EV aggregator power output and load disturbance, respectively; $D, M, R, \beta, F_p, T_g, T_r$ and T_c are the damping coefficient, generator inertia constant, speed drop, frequency bias factor, fraction of the total turbine power, time constant of the governor, reheat and turbine, respectively; and K_P and K_I are the PI controller gains.

The imbalance between demand and generation is measured in terms of incremental frequency variable Δf. The incremental variable is fed back to PI controller which sends appropriate control effect to the governor. The governor decides the valve opening of the turbine for increasing input of the synchronous generator. The constant action restores the imbalance between generator and demand. The fleet of Electric Vehicles called Ev aggregator connected through communication network and the conventional power system restores the frequency imbalance brought about by load variation. The load sharing between the conventional power system and EV aggregator is taken care using participation factors α_0 and α_1.

3.1.2 VARIABLE DESCRIPTION:

SL.NO:	VARIABLES	DESCRIPTION
1.	Δf	Deviation in frequency
2.	$\Delta\alpha_g$	Deviation in valve position
3.	ΔP_m	Deviation in mechanical power output
4.	ΔP_g	Deviation in generator power output
5.	ΔP_E	EV aggregator power output
6.	ΔP_d	Load disturbance

3.1.3 PARAMETER DESCRIPTION:

SL.NO:	PARAMETERS	DESCRIPTION
1.	D	Damping Coefficient
2.	M	Generator inertia constant
3.	R	Speed drop
4.	β	Frequency bias factor
5.	F_P	Fraction of total turbine power
6.	T_g	Governor Time Constant
7.	T_r	Reheat and Turbine Time Constant
8.	T_C	Generator Time Constant

3.1.4 CONTROLLER PARAMETERS AND PARTICIPATION FACTORS:

SL.NO:	PARAMETERS	DESCRIPTION
1.	K_P	Proportional gain
2.	K_I	Integral gain
3.	α_0	Participation Factor
4.	α_1	Participation factor of EV aggregator

3.1.5 EV AGGREGATOR PARAMETERS:

SL.NO:	PARAMETERS	DESCRIPTION:
1.	K_{EV}	Gain of EV aggregator
2.	T_{EV}	Time Constant of EV aggregator

For mathematical modeling purpose, the LFC system is illustrated as Fig.3.2,
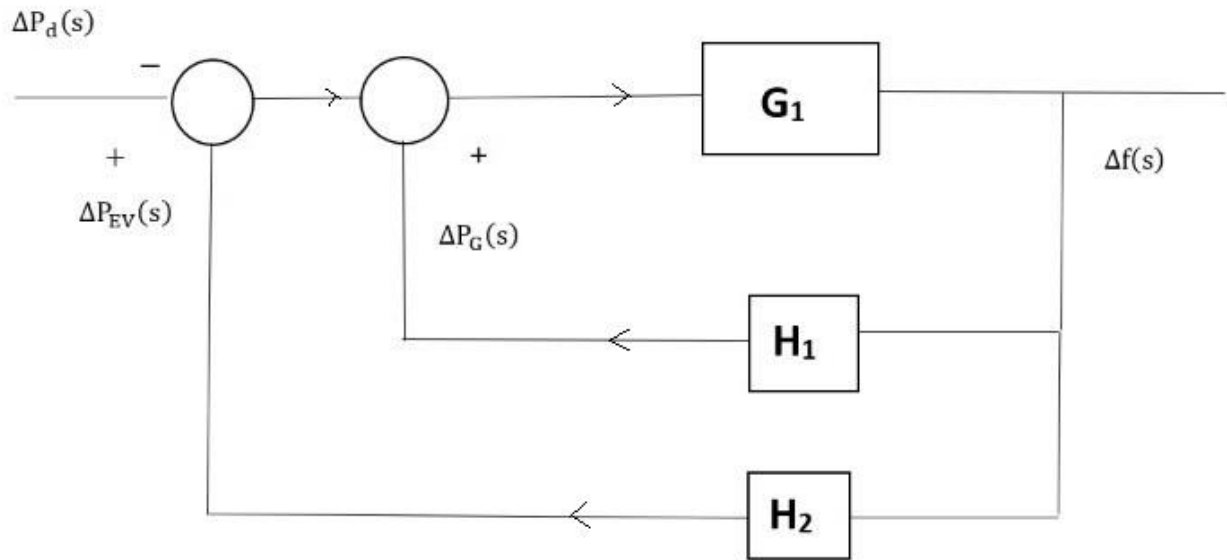
Let us consider,

$$G_1 = {}^1\!/\!(D + SM) \qquad (3.1)$$

$$H_1 = \frac{-[s[k_p\,\beta\alpha_0 R + 1] \; + k_I\beta\alpha_0 R][1 + SF_p T_r]}{Rs(1 + ST_g)(1 + ST_c)(1 + ST_r)}$$

$$H_2 = \frac{-[k_p\,\beta\alpha_1 k_{ev}\,s + k_2\beta\alpha_1 k_{ev}]e^{-s\tau}}{s + s^2 T_{EV}}$$

M=8.8; D=1 ; $\beta = 1$; $F_p = \frac{1}{6}$;
$T_{EV} = 0.1$; $T_g = 0.2$; $T_c = 0.3$; $T_r = 12$;
$K_{ev} = 1$; $K_p = 0.2$; $K_I = 0.6$;
$\alpha_0 = 0.8$; $\alpha_1 = 0.2$.

By using **signal flow graph method**, we find the transfer function of the System model of single-area LFC with EV aggregator.
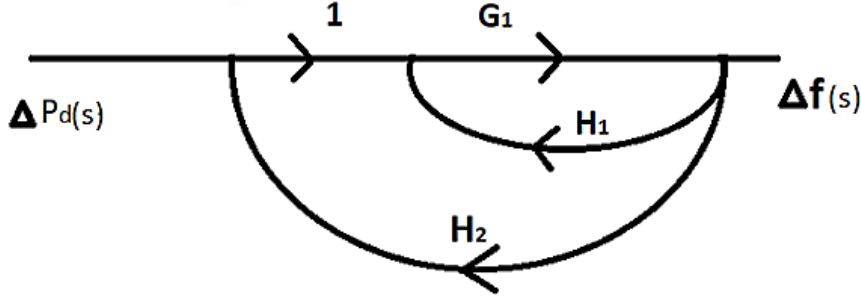
$$P_{1=}G_1; \quad \Delta_1 = 1 - 0 = 1.$$

$$L_{1=}G_1H_1. \quad ; \qquad L_{2=}G_1H_2 \; ; \qquad \Delta = 1 - [H_1 + H_2]G_1.$$

Maison's Gain formula:

Transfer function$= \dfrac{P_1\Delta_1}{\Delta}$.

$$= \frac{G_1 \times 1}{1 - G_1[H_1 + H_2]}$$

$$= \frac{\sfrac{1}{D+SM}}{1 + \frac{1}{D+SM}\left[\frac{[S(k_p \beta\alpha_0 R + 1] + k_I\beta\alpha_0 R][1 + SF_pT_r]}{Rs(1 + ST_g)(1 + ST_c)(1 + ST_r)} + \frac{-[k_p \beta\alpha_1 k_{ev} s + k_2\beta\alpha_1 k_{ev}]e^{-s\tau}}{s + s^2 T_{EV}}\right]}$$

$$= \frac{\sfrac{1}{D + SM}}{Rs(1 + ST_g)(1 + ST_r)(1 + ST_c)(D + SM)(s + s^2 T_{EV})] + [[s[k_p \beta\alpha_0 R + 1] + k_I\beta\alpha_0 R][1 + (1 + ST_r) - [k_p \beta\alpha_1 k_{ev} s + k_2\beta\alpha_1 k_{ev}]e^{-s\tau}}{(D + SM)(1 + ST_g)(1 + ST_c)(1 + ST_r)(s + s^2 T_{EV})}}$$

The closed loop transfer function of the time-delayed load frequency control system relates **Δf(s)**, the incremental frequency variable (output variable) to load

disturbance variable $\Delta P_d(s)$ (input variable).

The closed loop transfer function is derived as follows:

$$G(s) = \frac{\Delta f(s)}{\Delta P_{d(s)}} = \frac{N(s)}{P(s) + Q(s)e^{-s\tau}}$$

$N(s) = n_5 s^5 + n_4 s^4 + n_3 s^3 + n_2 s^2 + n_1 s^1 + n_0$
$= s^5[RT_{EV}T_R T_c T_g] + s^4[R[T_g T_R T_{EV} + T_R T_c T_{EV} + T_c T_g T_{EV} + T_R T_c T_g] + s^3[R[T_g T_{EV} + T_R T_{EV} + T_c T_{EV} + T_R T_g + T_R T_c + T_c T_g]] + s^2[R[T_R + T_g + T_c + T_{EV}]] + s[R]$

$P(s) = p_6 s^6 + p_5 s^5 + p_4 s^4 p_3 s^3 + p_2 s^2 + p_1 s^1 + p_0$
$= s^6[MRT_g T_r T_c T_{EV}] + s^5[DRT_g T_r T_c T_{EV} + MR(T_g T_r T_c + T_r T_c T_{EV} + T_g T_c T_{EV} + T_g T_r T_{EV})] + s^4[DR(T_g T_r T_c + T_r T_c T_{EV} + T_g + T_g T_r T_{EV}) + MR(T_r T_c + T_g T_c + T_g T_r + T_g T_{EV} + T_r T_{EV} + T_c T_{EV})] + s^3[DR(T_r T_c + T_g T_c + T_g T_r + T_g T_{EV} + T_r T_{EV} + T_c T_{EV}) + MR(T_r + T_c + T_g + T_{EV}) + F_p T_r T_{EV} + \alpha_0 \beta R K_p F_p T_r T_{EV}] + s^2[DR(T_r + T_c + T_g + T_{EV}) + MR + F_p T_r + T_{EV} + \alpha_0 \beta R(K_p T_{EV} + K_p T_r F_p + K_1 F_p T_r T_{EV})]$
$+ s^1[DR + 1 + \alpha_0 \beta R(K_p + k_1 T_{EV} + k_1 T_r F_p] + [\alpha_0 \beta R K_1]$

$Q(s) = \quad q_4 s^4 + q_3 s^3 + q s^2 + q_1 s^1 + q_0$

$= s^4[\alpha_1 \beta R K_{EV} K_p T_g T_r T_c] + s^3[\alpha_1 \beta R K_{EV}(K_p T_r T_c + K_p T_g T_c + K_p T_g T_r + K_1 T_g T_r T_c)] + s^2[\alpha_1 \beta R K_{EV}(K_p T_c + K_p T_g + K_p T_r + K_1 T_r T_c + K_1 T_g T_c + K_1 T_r T_g)] + s^1[\alpha_1 \beta R K_{EV}(K_p + K_1 T_c + K_1 T_r + K_1 T_g)] + [\alpha_1 \beta R K_{EV} K_1]$

For stability region and delay margin computations, it is necessary to obtain the characteristic equation of the single area LFC-EV system.

The characteristic equation of the single area LFC-EV system:

$$\Delta(s, \tau) = P(s) + Q(s)e^{-s\tau}$$

$\Delta(s, \tau) = \left[s^6[MRT_g T_r T_c T_{EV}] + s^5[DRT_g T_r T_c T_{EV} + MR(T_g T_r T_c + T_r T_c T_{EV} + T_g T_c T_{EV} + T_g T_r T_{EV})] + s^4[DR(T_g T_r T_c + T_r T_c T_{EV} + T_g T_c T_{EV} + T_g T_r T_{EV}) + MR(T_r T_c + T_g T_c + T_g T_r + T_g T_{EV} + T_r T_{EV} + T_c T_{EV})] + s^3[DR(T_r T_c + T_g T_c + T_g T_r + T_g T_{EV} + T_r T_{EV} + T_c T_{EV}) + MR(T_r + T_c + T_g + \right.$

T_{EV}) $+ F_p T_r T_{EV} + \alpha_0 \beta R K_p F_p T_r T_{EV}] + s^2[DR(T_r + T_c + T_{EV}) + MR + F_p T_r +$

$T_{EV} + \alpha_0 \beta R(K_p T_{EV} + K_p T_r F_p + K_1 F_p T_r T_{EV})] + s^1[DR + 1 + \alpha_0 \beta R(K_p +$

$k_1 T_{EV} + k_1 T_r F_p] + \qquad [\alpha_0 \beta R K_1]] \qquad + \qquad [s^4[\alpha_1 \beta R K_{EV} K_p T_g T_r T_c] +$

$s^3[\alpha_1 \beta R K_{EV}(K_p T_r T_c + K_p T_g T_c + K_p T_g T_r + K_1 T_g T_r T_c)] +$

$s^2[\alpha_1 \beta R K_{EV}(K_p T_c + K_p T_g + K_p T_r + T_r T_c + K_1 T_g T_c + K_1 T_r T_g)] +$

$s^1[\alpha_1 \beta R K_{EV}(K_p + K_1 T_c + K_1 T_r + K_1 T_g)] + [\alpha_1 \beta R K_{EV} K_1]] e^{-s\tau}.$

The roots of the characteristic equation are:

$0.05765 s^6 1.06734 s^5 + 6.02351 s^4 11.6329 s^3 + 7.20563 s^2 + 6.2595 s^1 + 1.145 = 0$

$S = -9.90431$

$S = -5.36025$

$S = -2.84345$

$S = -0.221403$

$S = -0.0923932 \pm 0.765317i$

The necessary condition for the single-area LFC-EV system to be asymptotically stable is that all the roots must be in the left half of the s-plane. In consideration of the single delay, the delay margin computation can be done by finding values of τ* for which has roots on the jω-axis. For some finite value of τ*, the characteristic polynomial of Δ (s, τ*) =0 has a root on the imaginary axis at s= $j\omega_c$, the equation of Δ (-s,τ*) =0 will also have the same root on the imaginary axis for the same value of τ* and ω_c due to the complex conjugate symmetry of complex roots. That means s= $j\omega_c$ will be a common root of the following equation:

$$\Delta(j\omega_c,, \tau^*) = P(j\omega_c) + Q(j\omega_c)e^{-jw_c\tau^*} = 0$$

$$\Delta(-j\omega_c, \tau^*) = P(-j\omega_c) + Q(-j\omega_c)e^{jw_c\tau^*} = 0$$

By eliminating the exponential terms between the above two sub-equations, the following augmented polynomial is obtained:

$W(\omega_c^2) = P(j\omega_c)P(-j\omega_c) - Q(j\omega_c) Q(-j\omega_c) = 0$

P(s)$=p_6s^6 + p_5s^5 + p_4s^4 + p_3s^3 + p_2s^2 + p_1s^1 + p_0.$

P(-s) $=p_6s^6 - p_5s^5 - p_4s^4 - p_3s^3 - p_2s^2 - p_1s^1 - p_0.$

⟶

(1)

P(s)×P(-s)

$= s^{12}p_6p_6 - s^{11}p_5p_6 + + s^{10}p_4p_6 - s^9p_3p_6 + s^8p_2p_6 - s^7p_1p_6 + s^6p_6p_0 +$

$s^{11}p_5p_6 + s^{10}p_5p_5 + s^9p_5p_4 - s^8p_5p_3 + s^7p_5p_2 - s^6p_5p_1 + s^{10}p_6p_4 - s^9p_5p_4 +$

$s^8p_4p_4 - s^7p_3p_4 + s^6p_2p_4 - s^5p_1p_4 + s^4p_0p_4 + s^9p_3p_6 - s^8p_3p_5 + s^7p_3p_4 -$

$s^5p_3p_2 - s^4p_3p_1 + s^3p_3p_0 + s^8p_6p_2 - s^7p_5p_2 + s^6p_4p_2 - s^5p_3p_2 -$

$s^4p_2p_2 - s^3p_1p_2 + s^2p_0p_2 + s^7p_6p_1 - s^6p_5p_1 + s^5p_4p_1 - s^4p_3p_1 + s^3p_2p_1 -$

$s^2p_1p_1 + s^1p_0p_1 + s^6p_6p_0 - s^5p_5p_0 + s^4p_4p_0 - s^3p_3p_0 + s^2p_2p_0 - s^1p_0p_1 + p_0^2.$

P(s)×P(-s) $= s^{12}p_6p_6 - s^{10}(p_5^2 - 2p_4p_6) + s^8(p_4^2 + 2p_2p_6 - 2p_5p_3) - s^6(p_3^2 +$

$2p_2p_4 + 2p_5p_1 - 2p_6p_0) + s^4(p_2^2 - 2p_3p_1 + 2p_4p_0) - s^2(p_1^2 - 2p_2p_0) + p_0^2.$

Q(s) $=q_4s^4 + q_3s^3 + q_2s^2 + q_1s^1 + q_0.$

Q(−s) $=q_4s^4 - q_3s^3 - q_2s^2 - q_1s^1 - q_0.$

(2)

Q(s)×Q(-s) $= s^8q_4^2 - s^7q_4q_3 + s^6q_4p_2 - s^5q_4q_1 + s^4q_3q_0 + s^7q_3q_4 - s^6q_3q_3 +$

$s^5q_3q_2 - s^4q_3q_1 + s^3q_3p_0 + s^6q_2q_4 - s^5q_3q_2 - s^4q_2q_2 - s^3q_2q_1 + s^2q_2q_0 +$

$s^5q_1q_4 - s^4q_3q_1 + s^3q_2q_1 + s^2q_2q_0 - s^1q_1q_0 + q_0^2.$

Q(s)×Q(-s) $= s^8q_4^2 - s^6(q_3^2 - 2q_4q_2) + s^4(q_2^2 + 2q_3q_0 + 2q_3q_1) - s^2 (q_1^2 - 2q_2q_0) + q_0^2.$

Substitute s = $j\omega_c$,

P(jω)×P(-jω)-Q(jω)×Q(-jω) $= \omega_c^{12}p_6^2 - \omega_c^{10}(p_5^2 - 2p_6p_4) + \omega_c^8(p_4^2 + 2p_2p_6 -$

$2p_5p_3) - \omega_c^6(p_3^2 + 2p_2p_4 + 2p_5p_1 - 2p_6p_0) + \omega_c^4 (p_2^2 - 2p_3p_1 + 2p_4p_0) - \omega_c^2(p_1^2 -$

$2p_2p_0) + p_0^2 - \omega_c^8q_4^2 + \omega_c^6(q_3^2 - 2q_4q_2) - \omega_c^4(q_2^2 + 2q_3q_0 - 2q_3q_1) + \omega_c^2(q_1^2 -$

$2q_2q_0) - q_0^2$

By substituting the polynomials of $P(j\omega_c)$, $P(-j\omega_c)$, $Q(j\omega_c)$ and $Q(-j\omega_c)$ into the augmented polynomial $W(\omega_c^2)$ of can be represented as

$$W(\omega_c^2) = t_{12}\omega_c^{12} + t_{10}\omega_c^{10} + t_8\omega_c^8 + t_6\omega_c^6 + t_4\omega_c^4 + t_2\omega_c^2 + t_0 = 0.$$

$$t_{12} = p_6^2.$$

$t_{10} = p_5^2 - 2p_6p_4$.

$t_8 = p_4^2 + 2p_6p_2 - 2p_5p_3 - q_4^2$.

$t_6 = p_3^2 - 2p_6p_0 - 2p_4p_2 + 2p_5p_1 - 2q_4q_2 - q_3^2$.

$t_4 = p_2^2 + 2p_4p_0 - 2p_3p_1 - 2q_4q_0 + 2q_3q_1 - q_2^2$.
$t_2 = p_1^2 - 2p_2p_0 + 2q_2q_0 - q_1^2$.

$t_0 = p_0^2 - q_0^2$.

$p_6 = 0.05765$;	$q_4 = 0.05497$;	$t_{12} = 0.003323$
$p_5 = 1.06734$;	$q_3 = 0.62764$;	$t_{10} = 0.4510$
$p_4 = 5.96854$;	$q_2 = 2.33573$;	$t_8 = 12.6955$
$p_3 = 11.0053$;	$q_1 = 2.9395$;	$t_6 = 69.828$
$p_2 = 4.8699$;	$q_0 = 0.2290$;	$t_4 = -40.217$
$p_1 = 3.320$;	$t_2 = -5.470$	
$p_0 = 0.916$;	$t_0 = 0.78661$	

W (ω_c^2) = 0

W (ω_c^2) = $0.00323\omega_c^2 + 0.451\omega_c^2 + 12.6955\omega_c^2 + 69.828\omega_c^2 - 40.217\omega_c^2 - 5.47\omega_c^2 + 0.786615 = 0$

$\omega_c^2 = -103.77$
$\omega_c^2 = -28.3095$
$\omega_c^2 = -8.06205$

$\omega_c^2 = -0.184679$
$\omega_c^2 = 0.091843$
$\omega_c^2 = 0.606242$

The real positive roots are $\omega_c = 0.3030561$ and $\omega_c = 0.7786154$. Calculating the

delay margin for each positive root and the minimum of those is taken as the

system delay marginτ^*.

The stability delay margin is $\tau^* = 0.6018600127$

COMPUTATION OF STABILITY REGIONS

To identify the boundary of the stability region in the parameter space of PI
controller, $(K_p - K_I)$-plane for a given time delay τ, s = $j\omega_c$ and the crossing
frequency $\omega_c >$ 0 is substituted into (2). The PI controller gains are then separated
to obtain a new equation as follows

P(s) = $\quad p_6 s^6 + p_5 s^5 + p_4 s^4 + p_3 s^3 + p_2 s^2 + p_1 s^1 + p_0$

$P(j\omega_c) = p_6\omega_c^6 + p_5 j\omega_c^5 + p_4\omega_c^4 - p_3 j\omega_c^3 - p_2\omega_c^2 + p_1\omega_c + p_0$
$P(j\omega_c) = [- p_6\omega_c^6 + p_4\omega_c^4 - p_2\omega_c^2 + p_0] + j[p_5\omega_c^5 - p_3 j\omega_c^3 + p_1\omega_c\}$
Q(s) = $\quad q_4 s^4 + q_3 s^3 + q s^2 + q_1 s^1 + q_0$
$Q(j\omega_c) = q_4\omega_c^4 - q_3 j\omega_c^3 - q_2\omega_c^2 + q_1\omega_c + q_0$
$Q(j\omega_c) = [q_4\omega_c^4 - q_2\omega_c^2 + q_0] + j [q_3\omega_c^3 + q_1\omega_c]$
$e^{-st} = e^{-j\omega_c t} = cos(\omega_c t) - j \, sin(\omega_c t)$
$P(j\omega_c) + Q(j\omega_c)e^{-j\omega_c t} = 0$
$[q_4\omega_c^4 - q_2\omega_c^2 + q_0] + j[q_3\omega_c^3 + q_1\omega_c] * cos(\omega_c t) - j \, sin(\omega_c t) = -P(j\omega_c)$
$[q_4\omega_c^4 - q_2\omega_c^2 + q_0] cos(\omega_c t) - [jq_4\omega_c^4 - q_2\omega_c^2 + q_0] sin(\omega_c t) + j[-q_3\omega_c^3 +$
$q_1\omega_c] * -j \, sin(\omega_c t) + j[-q_3\omega_c^3 + q_1\omega_c]cos(\omega_c t) =$
$-[P(j\omega_c) $ R $+ j P(j\omega_c)Q]$
$q_4\omega_c^4 - q_2\omega_c^2 + q_0] cos(\omega_c t) + [-q_3\omega_c^3 + q_1\omega_c] sin(\omega_c t) = P(j\omega_c)R$
$q_4\omega_c^4 - q_2\omega_c^2 + q_0] cos(\omega_c t) + [-q_3\omega_c^3 + q_1\omega_c] sin(\omega_c t) = -P(j\omega_c)R$
$q_4\omega_c^4 - q_2\omega_c^2 + q_0] cos(\omega_c t) - [-q_3\omega_c^3 + q_1\omega_c] sin(\omega_c t) = -P(j\omega_c)I$
$q_4' = K_p[\alpha_1\beta R K_{EV}T_g T_r T_c]$
$q_3' = [\alpha_1\beta R K_{EV}(K_p T_r T_c + K_p T_g T_c + K_p T_g T_r)]$
$q_3'' = K_I[\alpha_1\beta R K_{EV}T_g T_r T_c]$

$q_2' = \left[\alpha_1\beta RK_{EV}(K_pT_c + K_pT_g + K_pT_r)\right]$

$q_2'' = K_I\left[\alpha_1\beta RK_{EV}(T_rT_c + T_gT_c + T_gT_r)\right]$

$q_1' = \left[\alpha_1\beta RK_{EV}K_p\right]$

$q_1'' = K_I\left[\alpha_1\beta RK_{EV}T_gT_rT_c\right]$

$q_0'' = K_I\left[\alpha_1\beta RK_{EV}K_I\right]$

$p_6 = \left[MRT_gT_rT_cT_{EV}\right]$

$p_5 = \left[DRT_gT_rT_cT_{EV} + MR(T_gT_rT_c + T_rT_cT_{EV} + T_gT_cT_{EV} + T_gT_rT_{EV})\right]$

$p_4 = \left[DR(T_gT_rT_c + T_rT_cT_{EV} + T_gT_cT_{EV} + T_gT_rT_{EV}) + MR(T_rT_c + T_gT_c + T_gT_r \right.$
$\left. + T_gT_{EV} + T_rT_{EV} + T_cT_{EV})\right]$

$p_3 = \left[DR(T_rT_c + T_gT_c + T_gT_r + T_gT_{EV} + T_rT_{EV} + T_cT_{EV}) \right.$
$\left. + MR(T_r + T_c + T_g + T_{EV}) + F_pT_rT_{EV}\right]$

$p_3' = K_p\left[\alpha_0\beta RK_pF_pT_rT_{EV}\right]; p_2 = DR(T_r + T_c + T_g + T_{EV}) + MR + F_pT_r + T_{EV}$

$p_2' = K_p\left[\alpha_0\beta R[F_pT_r + T_{EV}]\right]; p_2'' = K_I\left[\alpha_0\beta RF_pT_rT_{EV}\right]$

$p_1 = DR+1$

$p_1' = K_p\left[\alpha_0\beta R[+1]\right]$

$p_1'' = K_I\left[\alpha_0\beta R[F_pT_r + T_{EV}]\right]$

$p_0'' = K_p\left[\alpha_0\beta R\right]$

$q_4\omega_c^4 - q_2\omega_c^2 + q_0]\cos(\omega_ct) + [-q_3\omega_c^3 + q_1\omega_c]\sin(\omega_ct) = -[-p_6\omega_c^6 + p_4\omega_c^4 - p_2\omega_c^2 + p_0].$

$[-q_3\omega_c^3 + q_1\omega_c]\cos(\omega_ct) - q_{+4}\omega_c^4 - q_2\omega_c^2 + q_0]\sin(\omega_ct) = -[p_5\omega_c^5 - p_3j\omega_c^3 + p_1\omega_c]$

REAL PART

$k_p[[q_4'\omega_c^4 - q_2'\omega_c^2]\cos(\omega_c + 1)\ [-q_3'\omega_c^3 - q_1'\omega_c]\sin(\omega_c + 1)]$

$k_I[[-q_2''\omega_c^2 + q_0'']\cos(\omega_c + 1)\ [-q_3''\omega_c^3 - q_1''\omega_c]\sin(\omega_c + 1)]$

$= [-p_6\omega_c^6 + p_4\omega_c^4 - p_2\omega_c^2 k_p[-p_2'\omega_c^2]\ k_I[[-p_2''\omega_c^2 + p_0''].$

$k_p[-p_2'\omega_c^2 + q_4'\omega_c^4\cos(\omega_c + 1) - q_2'\omega_c^2\cos(\omega_c + 1) - q_3'\omega_c^3\sin(\omega_c + 1)$

$+q_1'\omega_c\sin(\omega_c + 1)] + k_I[-p_2''\omega_c^2 + p_0'' - q_2''\omega_c^2\cos(\omega_c + 1) + q_0''\cos(\omega_c + 1) -$

$q_3''\omega_c^3\sin(\omega_c + 1) + q_1''\omega_c\sin(\omega_c + 1)] + [p_6\omega_c^6 - p_4\omega_c^4 + p_2\omega_c^2].k_pA_1(\omega_c) +$

$k_IB_1(\omega_c) = -C_1(\omega_c)$

IMAGINARY PART

$k_p[-q_3'\omega_c^4]\cos(\omega_ct) + [q_4'\omega_4^3 + q_2'\omega_c^2]\sin(\omega_ct)] + k_I[[-q_3''\omega_c^2]\cos(\omega_ct)$

$[+q_1''\omega_c - q_1''\omega_c\cos(\omega_ct)] + [-q_2''\omega_c^2 - q_0'']\sin(\omega_ct)]$

$= -[p_5\omega_c^5 - p_3j\omega_c^3 + p_1\omega_c k_p[-p_3'\omega_c^3 + p_1'\omega_c^3]\ k_I[[p_1''\omega_c]]$

$$k_p[-p_3'\omega_c^3 + p_1'\omega_c - q_3''\omega_c^3\,cos(\omega_c t) + q_4'\omega_c^4 sin(\omega_c t) + q_2'\omega_c^2 sin(\omega_c t) +$$
$$k_I[p_1''\omega_c - q_3''\omega_c^3\,cos(\omega_c t) + q_1''\omega_c^2\,cos(\omega_c t) + q_2''\omega_c^2 sin(\omega_c t) - q_0''\omega_c sin(\omega_c t)]$$
$$=[-p_5\omega_c^5 - p_3\omega_c^3 - p_1\omega_c]$$

$k_p A_2(\omega_c) + k_I B_2(\omega_c) = -C_2(\omega_c)$ $\longrightarrow$ (3)

$k_p A_2(\omega_c) + k_I B_2(\omega_c) + C_2(\omega_c) = 0$ $\longrightarrow$ (4)

From 3 and 4 we get

$$k_p = \frac{B_1(\omega_c)C_2(\omega_c) - B_2(\omega_c)C_1(\omega_c)}{A_1(\omega_c)B_2(\omega_c) - A_2(\omega_c)B_1(\omega_c)} \to (5)$$

From 3 and 4 we get

$$k_p = \frac{A_2(\omega_c)C_1(\omega_c) - A_1(\omega_c)C_2(\omega_c)}{A_1(\omega_c)B_2(\omega_c) - A_2(\omega_c)B_1(\omega_c)} \to (6)$$

$K_p A_1(\omega_c) + K_I B_1(\omega_c) + C_1(\omega_c) = 0$

$K_p A_2(\omega_c) + K_I B_2(\omega_c) + C_2(\omega_c) = 0$ $\qquad \longrightarrow$ (7)

The coefficients are

$A_1(\omega_c) = -p'_2\omega_c^2 + q'_4\omega_c^4 cos(\omega_c t) - q'_2\omega_c^2 cos(\omega_c t) - q'_3\omega_c^3 sin(\omega_c t) + q'_1\omega_c sin(\omega_c t)$

$B_1(\omega_c) = -p''_2\omega_c^2 + p''_0 - q''_2\omega_c^2 cos(\omega_c t) + q''_0 cos(\omega_c t) - q''_3\omega_c^3 sin(\omega_c t) + q''_1\omega_c sin(\omega_c t)$

$C_1(\omega_c) = -p\omega_c^6 + p\omega_c^4 - p_2\omega_c^2$

$A_2(\omega_c) = -p'_3\omega_c^3 + p'_1\omega_c - q'_3\omega_c^3 cos(\omega_c t) + q'_4\omega_c^4 sin(\omega_c t) + q'_2\omega_c^2 sin(\omega_c t)$

$B_2(\omega_c) = p''_1\omega_c - q''_3\omega_c^3 cos(\omega_c t) + q''_1\omega_c cos(\omega_c t) + q''_2\omega_c^2 sin(\omega_c t) - q''_0 sin(\omega_c t)$

$C_2(\omega_c) = p_5\omega_c^5 - p_3\omega_c^3 + p_1\omega_c$

It should be noted that p_6, p_5 and p_4 coefficients in the above equations are those given in (1) and q_3, q_4 and q_3 coefficients in the above equations are those given in (2) on the other hand the coefficients of p'' and q'' in the above equations corresponds to the remaining terms of p and q containing K_I, respectively. The stability boundary obtained by (10) is called as complex root boundaries (CRBs) of the LFC-EV system. It is noted that a real root may cross the jω axis origin. Moreover, it can be observed that such a stability change occurs only for $K_I=0$, defining another boundary called as Real Root Boundary (RRB) locus. As a result, the (K_P, K_I)-plane is divided into stable and unstable regions by the RRB locus $K_I = 0$ and the CRB locus, obtained by (7) which will be discussed next chapter.

CHAPTER 4: SIMULATIONS ANDRESULTS

4.1.0 DELAY DEPENDENT STABILITY:

Computation of stability delay margin:

The objective is to compute the maximum value of the delay (τ^*) within which the closed loop system remains asymptotically stable. In this problem, all the load frequency control system parameters are known and The PI controller parameters K_p and K_I are assumed to be known.

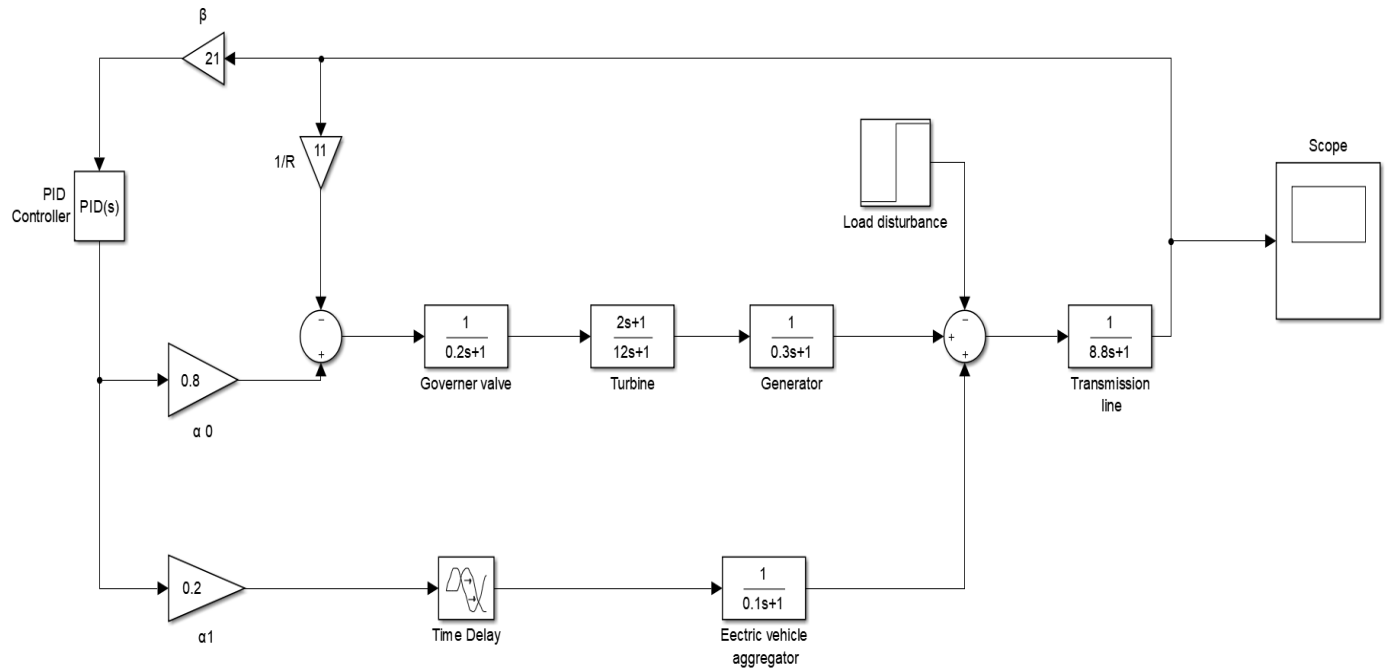**Simulink Model of Single Area LFC control system with EV aggregator:**

Fig 4.1 Simulink Model of Single Area LFC control system with EV aggregator.

4.1.1 BENCHMARK SYSTEM PARAMETERS:

SL.NO	PARAMETERS	DESCRIPTION	VALUE
1.	M	Generator inertia constant	8.8
2.	D	Damping Coefficient	1
3.	T_g	Governor Time Constant	0.2
4.	T_C	Generator Time Constant	0.3
5.	T_r	Reheat and Turbine Time Constant	12
6.	F_P	Fraction of total turbine power	1/6
7.	R	Speed drop	1/11
8.	β	Frequency bias factor	21
9.	K_{EV}	Gain of EV aggregator	1
10.	T_{EV}	Time Constant of EV aggregator	0.1

Table 4.1 Parameters of LFC system.

These are the benchmark parameters used to compute the maximum value of the delay (τ^*) within which the closed loop system remains asymptotically stable.

 The MATLAB program to compute the stability delay margin is given below,

4.1.2 MATLAB code for computation of stability delay margin:

clear ALL

M= 8.8;
D= 1;

```
Tg=   0.2;
Tc=   0.3;
Tr=   12;
Fp=   1/6;
R=    1/11;
Beta= 21;
Kev= 1;
Tev= 0.1;

alpha0= 0.8;
alpha1= 0.2;

Ki = 0.6;
Kp = 0.2;
p6= (M*R*Tg*Tr*Tc*Tev);
p5= (D*R*Tg*Tr*Tc*Tev) + (M*R) *(Tg*Tr*Tc + Tr*Tc*Tev + Tg*Tc*Tev +
Tg*Tr*Tev);
p4= (D*R) *(Tg*Tr*Tc + Tr*Tc*Tev + Tg*Tc*Tev + Tg*Tr*Tev) + (M*R) *(Tr*Tc +
Tg*Tc + Tg*Tr + Tc*Tev + Tg*Tev+ Tr*Tev);
p3= (D*R) *(Tc*Tr+ Tg*Tc + Tg*Tc + Tg*Tr + Tc*Tev + Tr*Tev + Tg*Tev) + (M*R)
*(Tc+Tr+Tg+Tev) +(Fp*Tr*Tev) + (alpha0*Beta*R*Kp*Fp*Tr*Tev);
p2= (D*R) *(Tc+Tr+Tg+Tev) +(M*R) +(Fp*Tr) +Tev+(alpha0*Beta*R) *(Kp*Tev +
Kp*Fp*Tr + Ki*Fp*Tr*Tev);
p1= (D*R) + 1 + (alpha0*Beta*R) *(Kp+ Ki*Tev + Ki*Fp*Tr);
p0= (alpha0*Beta*R*Ki);

q4= (alpha1*Beta*R*Kev*Kp*Tg*Tr*Tc);
q3= (alpha1*Beta*R*Kev) *(Kp*Tr*Tc + Kp*Tg*Tc + Kp*Tg*Tr + Ki*Tg*Tc*Tr);
q2= (alpha1*Beta*R*Kev) *(Kp*Tc + Kp*Tr + Kp*Tg + Ki*Tr*Tc + Ki*Tg*Tc
+Ki*Tg*Tr);
q1= (alpha1*Beta*R*Kev) *(Kp + Ki*Tc + Ki*Tr + Ki*Tg);
q0= alpha1*Beta*R*Kev*Ki;
t12= p6^2;
t10= p5^2 - 2*p6*p4;
t8 = p4^2 + 2*p6*p2 - 2*p5*p3 - q4^2;
t6 = p3^2 - 2*p6*p0 - 2*p4*p2 + 2*p5*p1 + 2*q4*q2 - q3^2;
t4 = p2^2 + 2*p4*p0 - 2*p3*p1 - 2*q4*q0 + 2*q3*q1 - q2^2;
```

```
t2 = p1^2 - 2*p2*p0 + 2*q2*q0 - q1^2;
t0 = p0^2 - q0^2;

k=1;
r = roots ([t12 t10 t8 t6 t4 t2 t0]);
for i=1: size(r,1)
   an(i)=angle(r(i)) *(180/pi);
   if (an(i)==0)
      w1(k)=r(i);
      k=k+1;
   end
end

m = 0;
for n = 1: size(w1,2)
   wa (: n) = sqrt (w1(: n));
   wc = wa (: n);
   derWc = 6*t12*wc^10 + 5*t10*wc^8 + 4*t8*wc^6 + 3*t6*wc^4 + 2*t4*wc^2 +
t2;
RT = sign(derWc);
   if(RT==1)
      m = m+1;
      P = p6*(j*wc) ^6 + p5*(j*wc) ^5 + p4*(j*wc) ^4 + p3*(j*wc) ^3 + p2*(j*wc) ^2
+ p1*(j*wc) ^1 + p0;
      Q = q4*(j*wc) ^4 + q3*(j*wc) ^3 + q2*(j*wc) ^2 + q1*(j*wc) ^1 + q0;
      SIN = imag(P/Q);
      COS = real(-P/Q);
      theta = atan(SIN/COS);
      if COS<0
         tau1(:m) = ((theta+pi)/wc);
      else
         tau1(:m) = (theta/wc);
      end
      RT;
      wc;
      tau1;
   else
```

```
        RT;
        wc;
    end
end
Kp
Ki
format long g
tau = min(tau1)
format
```
The result of the above-mentioned MATLAB code is:

```
>> LFCS

Kp =

      0.2000


Ki =

      0.6000


tau =

          0.601860012708232
```

4.1.3 MATLAB output for different $K_p$and $K_I$values:

τ^* - STABILITY DELAY MARGIN (s)

K_p	K_I=0.2	K_I=0.4	K_I=0.6	K_I=0.8	K_I=1.0
0	1.7866	0.4231	0.0859	-0.0615	-0.1417
0.1	2.7421	0.8271	0.3496	0.1340	0.0134
0.2	3.5861	1.2002	**0.6018**	0.3242	0.1656
0.3	4.2522	1.5214	0.8327	0.5034	0.3115
0.4	4.6970	1.7773	1.0346	0.6669	0.4477
0.5	4.8537	1.9635	1.2023	0.8108	0.5717
0.6	4.6817	2.0829	1.3339	0.9327	0.6812
0.7	4.3135	2.1433	1.4300	1.0317	0.7751
0.8	3.9050	2.1545	1.4932	1.1080	0.8527
0.9	3.5197	2.1273	1.5275	1.1628	0.9142
1.0	3.1740	2.0715	1.5372	1.1982	0.9606

Table 4.2 stability delay margin for various K_p and K_I values.

4.1.4 SIMULATION RESULTS:

Stability analysis for various communication delays. This simulation results shows the impact of communication delay in the load frequency control system integrated with electric vehicle aggregator.

1.For K_p=0.2, K_I=0.6 and Communication Delay, τ^*= 0.6018 sec

Marginal stable response:
In this, the frequency response exhibits sustained oscillations which indicate the marginal stability of LFC-EV system.
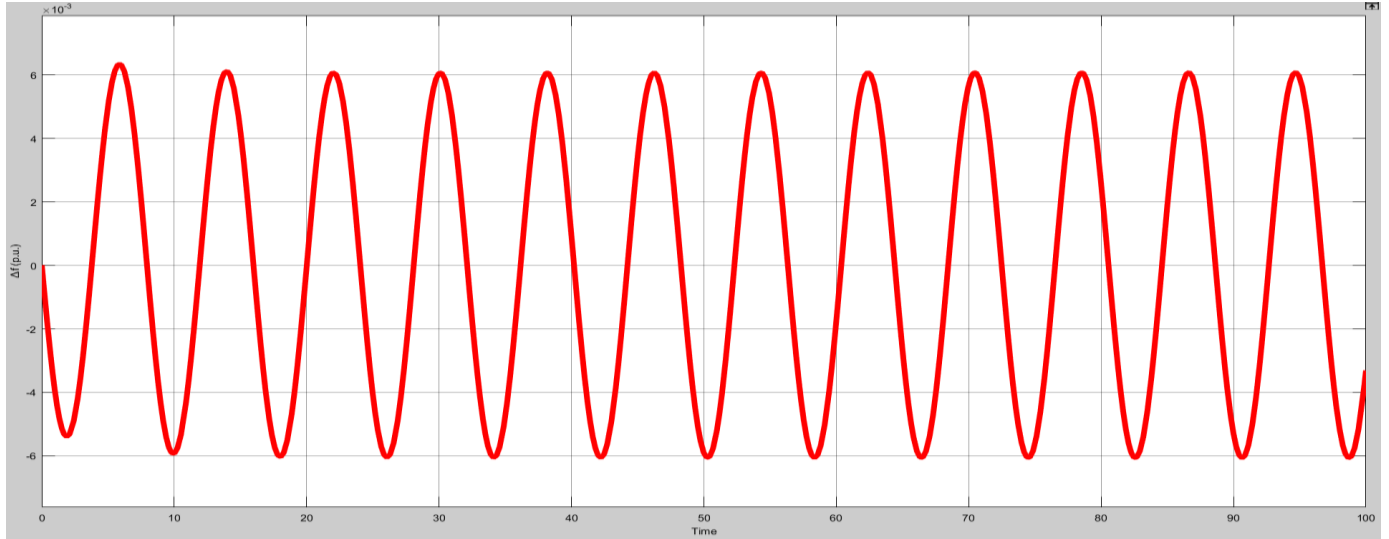
Fig 4.1 the plot of incremental frequency vs time for $\tau^* = 0.6018$ sec

1. **For K_p=0.2,K_I=0.6 and Communication Delay, τ^*= 0.5751sec**

   Stable response:
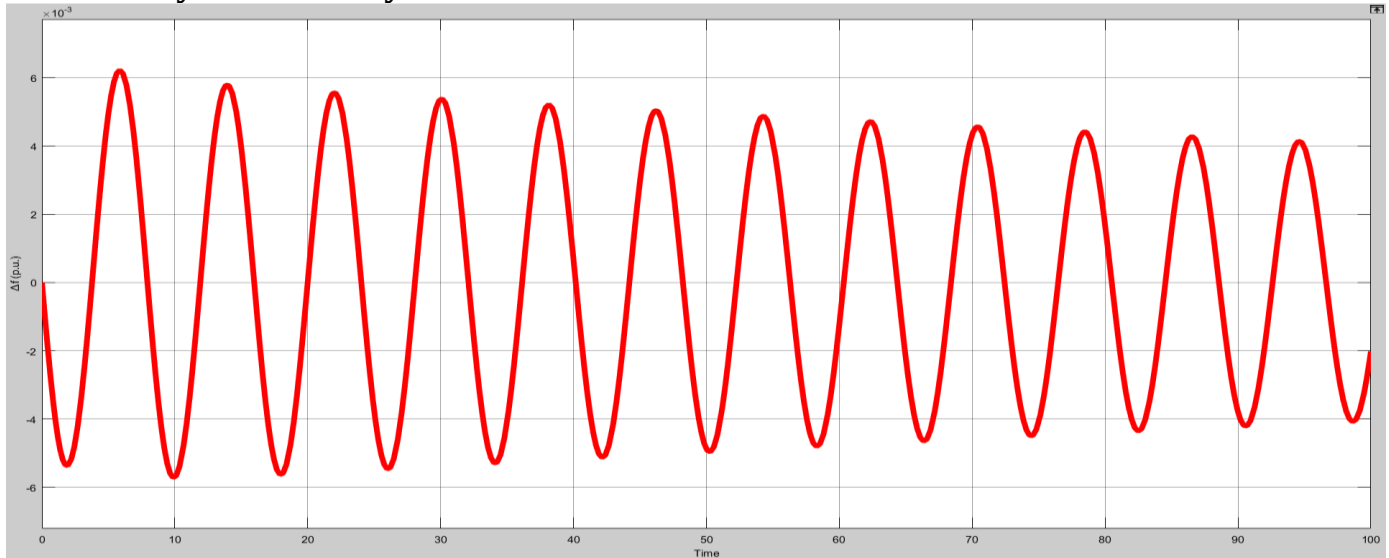In this, the frequency response exhibits decaying oscillations which indicate the stability of LFC-EV system.

Fig 4.2 the plot of incremental frequency vs time for τ^*= 0.5751sec

3. For K_p=0.2,K_I=0.6 and Communication Delay, τ^*= 0.6252 sec

Unstable response:
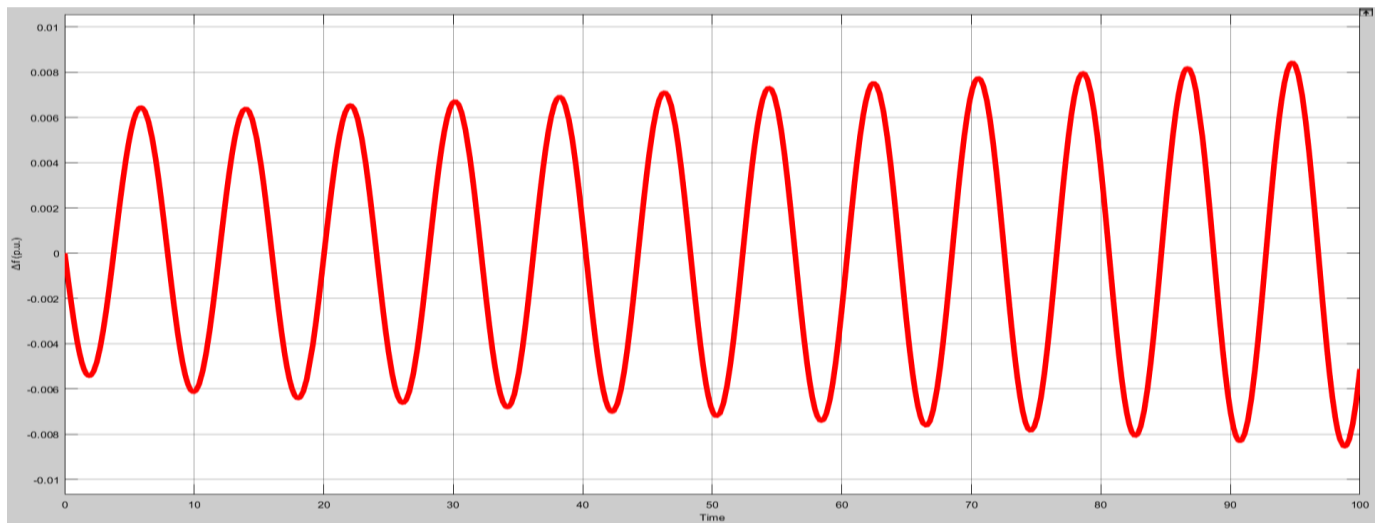In this, the frequency response exhibits growing oscillations which indicate the instability of LFC-EV system.

Fig 4.3 the plot of incremental frequency vs time for $\tau^* = 0.6252$ sec

4.2.0 COMPUTATION OF STABILITY DELAY MARGINS:

The objective is to compute a feasible origin in PI controller parametric space. In this problem, all the LFC system parameters except controller parameters are known. The time-delay in the communication network is assumed to be known.

The MATLAB program to compute the stability delay regions is given below,

4.2.1 MATLAB CODE FOR COMPUTATION OF STABILITY REGIONS:

```
Clear all
M=8.8;
D=1;
Tg=0.2;
Tc=0.3;
Tr=12;
Fp=1/6;
R=1/11;
beta=21;
Kev=1;
```

```
Tev=0.1;
alpha1=0.1;
alpha0=0.9;
Q4=Kp*[alpha1*beta*R*Kev*Tg*Tr*Tc];
Q3= Kp*[alpha1*beta*R*Kev*[Tr*Tc+Tg*Tc+Tg*Tr]];
Qq3=Ki*[alpha1*beta*R*Kev*Tg*Tr*Tc];
Q2=Kp*[alpha1*beta*R*Kev*[Tc+Tr+Tg]];
Qq2=Ki*[alpha1*beta*R*Kev*[Tr*Tc+Tc*Tg*Tc+Tg*Tr];
Qq0=Ki*[alpha1*beta*R*Kev*Ki];
Q1=Kp*[alpha1*beta*R*Kev];
Qq1=Ki*[alpha1*beta*R*Kev*[Tc+Tr+Tg]];
p6=M*R*Tg*Tr*Tc*Tev;
p5=D*R*Tg*Tc*Tr*Tev+M*R*[Tg*Tr*Tc+Tr*Tc*Tev+Tg*Tc*Tev+Tg*Tr*Tev];
p4=D*R*[Tr*Tg*Tc+Tr*Tc*Tev+Tg*Tc*Tev+Tg*Tr*Tev]+M*R*[Tr*Tc+Tg*Tc+Tg*Tr
+Tc*Tev+Tr*Tev+Tg*Tev];
p3=D*R*[Tr*Tc+Tg*Tc+Tg*Tr+Tc*Tev+Tr*Tev+Tg*Tev]+M*R*[Tc+Tr+Tg+Tev]+Fp*
Tr*Tev;
P3=Kp*[alpha0*beta*R*Fp*Tr*Tev];
p2=D*R*[Tc+Tr+Tg+Tev]+M*R+Fp*Tr+Tev;
P2=Ki*[alpha0*beta*R*[Tev+Fp*Tr]];
Pp2=Ki*[alpha0*beta*R*Fp*Tr*Tev];
p1=D*R+1;
P1=Kp*[alpha0*beta*R+1];
Pp1=Ki*[alpha0*beta*R*[Tev+Fp*Tr]];
Pp0=Ki*[alpha0*beta*R];
t = 0.5;
wc = 0:0.01:3.91;
for i=1:size(wc,2)
   A1(:,i) = -P2*wc^2+Q4*wc^2*cos(wc*t)-Q2*wc^2*cos(wc*t)-
Q3*wc^3*sin(wc*t)+Q1*wc*sin(wc*t);
   B1(:,i) = -Pp2*wc^2+Pp0-Qq2*wc^2*cos(wc*t)+Qq0*cos(wc*t)-
Qq3*wc^3*sin(wc*t)+Qq1*wc*sin(wc*t);
   A2(:,i) = -P3*wc^3+P1*wc-
Q3*wc^3*cos(wc*t)+Q4*wc^4*sin(wc*t)+Q2*wc^2*sin(wc*t);
   B2(:,i) = Pp1*wc-
Qq3*wc^3*cos(wc*t)+Qq1*wc*cos(wc*t)+Qq2*wc^2*sin(wc*t)-Qq0*sin(wc*t);
   C1(:,i) = -p6*wc^6+p4*wc^4-p2*wc^2;
```
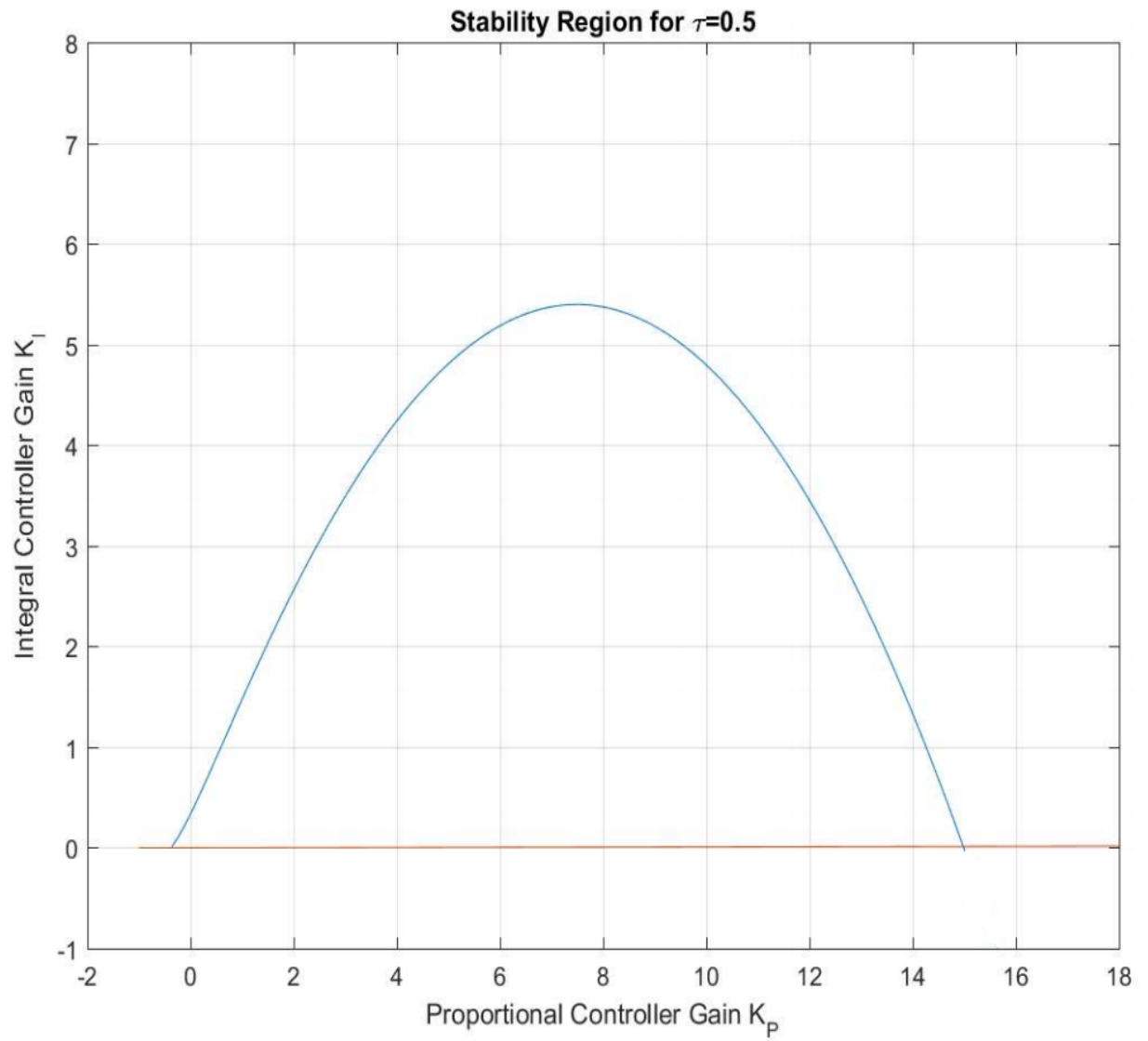
```
    C2(:,i) = p5*wc^5-p3*wc^3+p1*wc;
    Kp(:,i) = (B1(:,i)*C2(:,i)-B2(:,i)*C1(:,i))/(A1(:,i)*B2(:,i)-A2(:,i)*B1(:,i));
    Ki(:,i) = (A2(:,i)*C1(:,i)-A1(:,i)*C2(:,i))/(A1(:,i)*B2(:,i)-A2(:,i)*B1(:,i));
end
end
plot(Kp, Ki)
hold on

x = 0;
y = -0.03:0.0001:0.059;
plot(y,x,'k')
grid
axis([-0.04 0.07 -0.02 0.12])
xlabel ('Proportional Controller Gain K_{P}')
ylabel ('Integral Controller Gain K_{I}')
title ('Stability Region for \tau=0.5')
```

The result of the above-mentioned MATLAB code is:

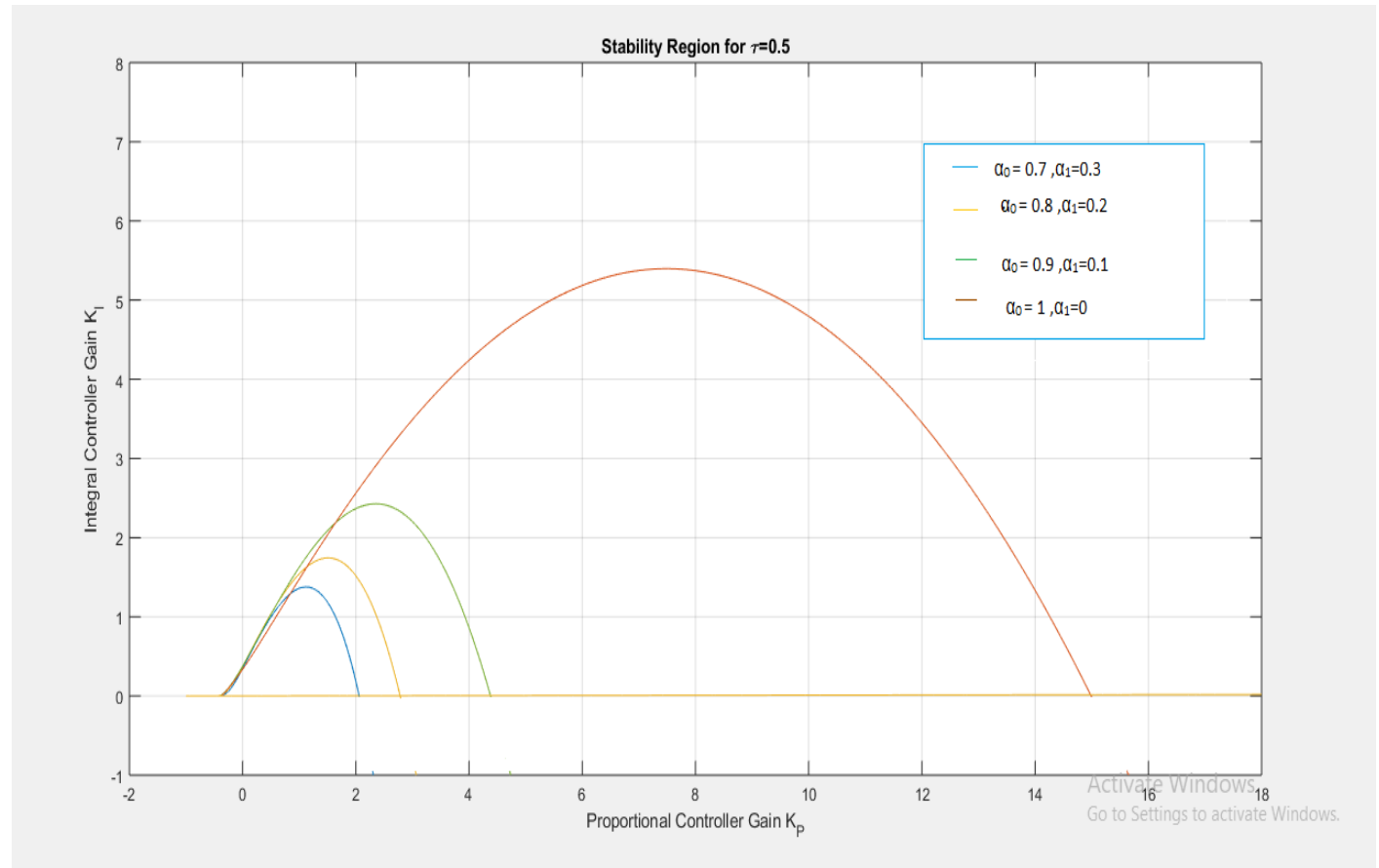## 4.2.2 STABILITY REGION CURVE FOR TIME DELAY=0.5s FOR VARIOUS PARTICIPATION FACTORS:

Fig 4.4 The plot of integral controller gain K_I vs proportional controller gain K_p.

1. **For system to be stable:** The values of K_p and K_I should lie within the curve boundary for that participation factors.
   Example: For α_1=0.3 and α_0=0.7 the values are K_p =1 and K_I =0.5.
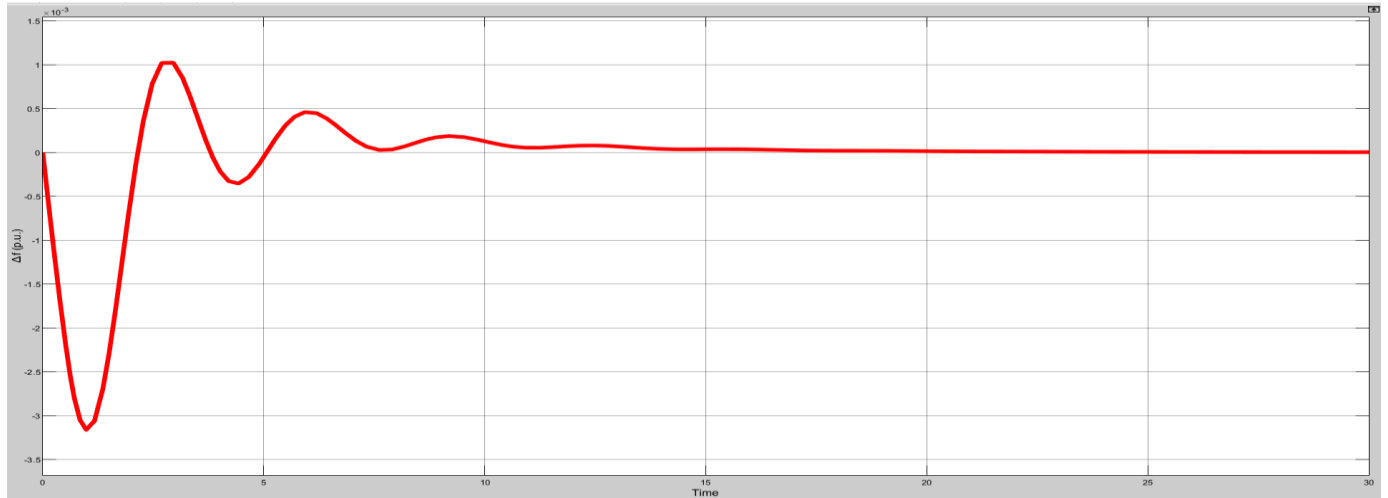
Fig 4.5The plot of incremental frequency vs time for K_p =1 and K_I =0.5.

2. **For system to be unstable:** The values of K_p and K_I should lie anywhere out of curve boundary for that particular participation factors.

   Example: For α_1=0.3 and α_0=0.7, the values are K_p =3 and K_I =2.
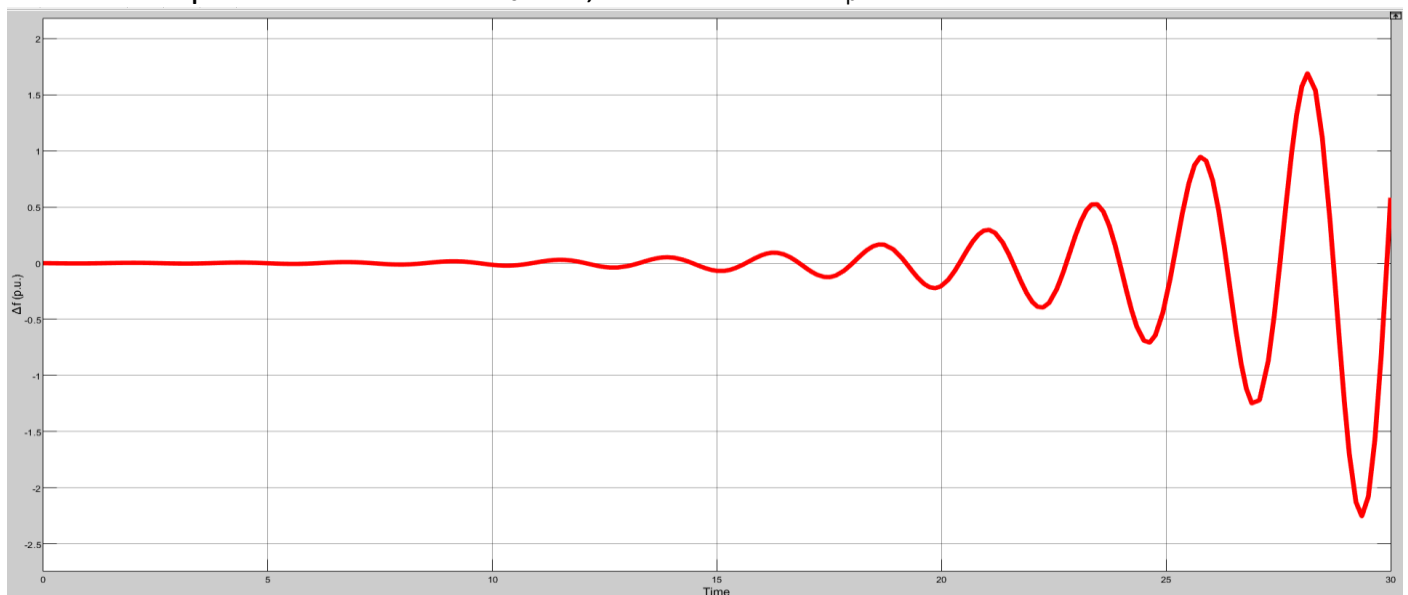

Fig 4.6The plot of incremental frequency vs time for K_p =3 and K_I =2.

3. **For system to be marginally stable:** The values of K_p and K_I should lie on or near to the curve boundary for that particular participation factors.

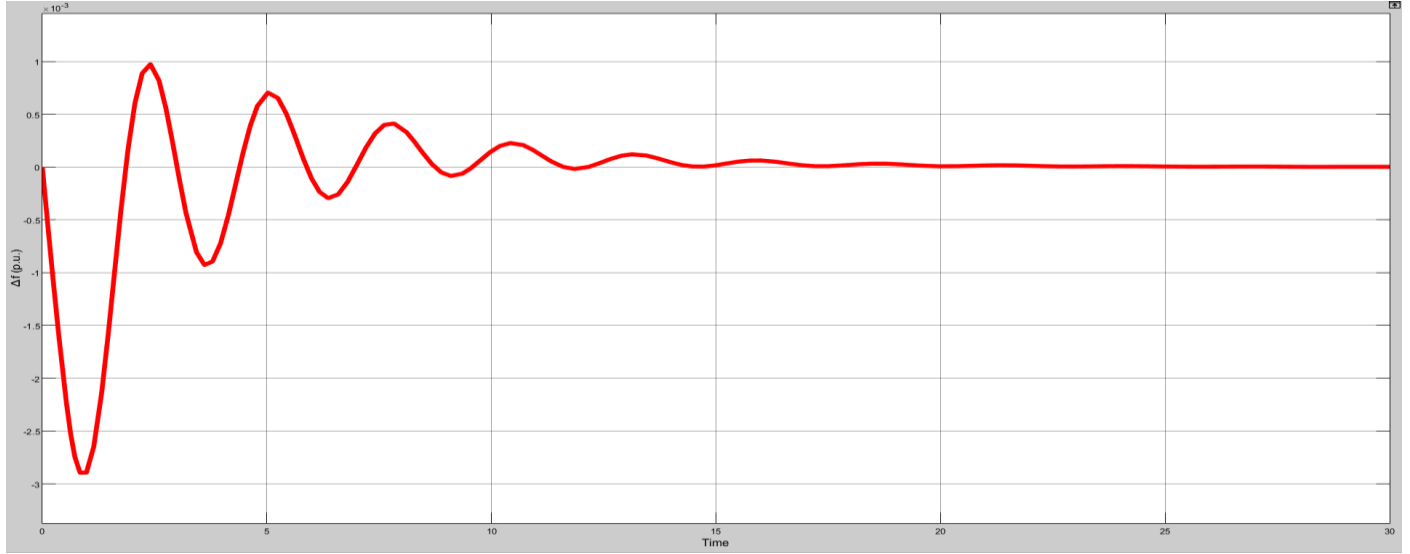   Example: For α_1=0.3 and α_0=0.7, the values are K_p =1.8 and K_I =1.4.

Fig 4.7 The plot of incremental frequency vs time for K_p =1.8 and K_I =1.4.

4.3.0 CONCLUSION:

Stability delay margins are computed for a wide range of PI controller gains. The stability delay margins are shown in Table 4.1 for EV participation factor of α_1 = 0.2. The results in Table 4.1 indicate that for a fixed value of K_P, the stability delay margin decreases when K_I is increased, which infers a less stable system. The stability delay margin increases with $K_P$for nearly all values of K_I. The theoretical delay margins are verified using timedomain simulations. The frequency response exhibits sustained oscillations which indicate the marginal stability of LFC-EV system. If the time delay exceeds the stability delay margin, the system will become unstable due to the growing oscillations in the frequency response. The stability region in the (K_P, K_I)-plane is obtained for without EV aggregator and with three different EV aggregator participation factorsα_1 = 0.1, 0.2 and 0.3, whereas the time delay is fixed at τ = 0.5 s. These participation factors imply that 10%, 20% and 30% of the required control efforts are provided by the EV aggregator with a time delay of τ = 0.5 s. Figure 4.4 compares the corresponding stability regions. Note that the largest region is observed when EV participation is

49

not considered (α_1 = 0). More importantly, the size of stability regions decreases as the EV participation factor increases, whereas the shape of the regions is unchanged. Figure 4.4 clearly illustrates that the stability regions get smaller as the contribution of EV aggregator to the frequency regulation increases due to the presence of communication time delay. The accuracy of stability boundary locus is validated by the time-domain simulations. It can be seen that the LFC-EV system is marginally stable due to undamped frequency response because of a complex conjugate root pair located on the jω-axis for the selected gains. This implies that the LFC-EV system will be asymptotically stable with decaying oscillation in the frequency response for any PI controller gains inside the region. The LFC-EV system will become unstable with growing oscillations in frequency for any controller gains outside the region.

Chapter 5: Conclusion

   This project work has presented a comprehensive study on the effect of integrating EV aggregator with communication time delay to conventional LFC system. For a given time delay and load sharing scheme, a set of all stabilizing PI controller gains that constitute a stability region in the parameter space of the controller have been determined using a graphical exact method. The impact of both time the delay and EV aggregator participation factor on the stability regions has been evaluated. It is observed that the size of stability regions decreases as the time delay and EV participation factor increase.

   To complement stability region results, stability delay margins have been determined for a large number of PI controller gains using a frequency domain exact method. It has been observed that stability delay margin becomes smaller with an increase in the integral gain. Moreover, for any given PI controller gains, an increase in EV aggregator participation factor results in a decrease in stability delay margin. If the PI controller gains and participation factor of EVs are not properly selected, the participation of EV aggregator with a communication time delay may cause instability and degrade the dynamic response against an expectation that EVs can improve the LFC dynamic performance.

   It is expected that the results will allow us to determine the communication delay requirements and the design of PI controller for EV aggregators participating in frequency regulation service. In the future, the gain and phase margins will be taken into account for obtaining stability regions of load frequency control systems with multiple EVs aggregators and time delays to calculate all possibly purely complex roots and imaginary roots of characteristics equation. Also, the stability regions will be computed for multi-area load frequency control system. Along with that, computation of relative stability specifications will be included.

Chapter 6: References and Base Paper

1) Ausnain Naveed Sahin Sonmez and Saffet Ayasun,'Impact of Electric Vehicle Aggregator with communication Time delay on Stability Regions and Stability Delay Margins in Load Frequency control System', Journal of Modern Power Systems and clean Energy, In press, DOI: 10.35833/MPCE.2019,Springer**. (BASE PAPER).**

2) Hakan Gunduz, Sahin Sonmez and Saffet Ayasun, 'Impact of Electric Vehicles Aggregator on the Stability Region Micro-Grid System with Communication Time Delay,' 2019 IEEE Milan Power Tech.

3) Vijay P. Singh, Nand Kishor, and Paulson Samuel, 'Communication Time Delay Estimation for Load Frequency Control in Two Area Power Systems,' *Ad Hoc Networks*, Vol. 41, No. 1, pp. 69-85, May 2016.

4) Ausnain Naveed, Sahin Sonmez and Saffet Ayasun, 'Stability Regions in the Parameter Space for LFC System with EV Aggregator and Incommensurate Time Delays,' 1st IEEE Global Power Energy and Communication Conference (GPECOM 2019), June 12-15, 2019, Cappadocia, Turkey.

5) Han, Y., Zhang, K., Hong, L., Coelho, E. A. A., and Guerrero, J. M, 'MAS-based Distributed Coordinated Control and Optimization in Microgrid and Microgrid Clusters: A Comprehensive Overview.' *IEEE Transactions on Power Electronics*, Vol. 33, No. 8, pp. 6488-6508, 2018.

6) H. Luo, I. A. Hiskens and Z. Hu, 'Stability Analysis of Load Frequency Control Systems With Sampling and Transmission Delay,' *IEEE Transactions on Power Systems*, Vol. 35, No. 5, pp. 3603-3615, Sept. 2020

7) K. S. Ko and D. K. Sung, 'The Effect of EV Aggregators With Time-Varying Delays on the Stability of a Load Frequency Control System,' *IEEE Transactions on Power Systems*, Vol. 33, No. 1, pp. 669-680, Jan. 2018

8) Deniz Katipoglu, Sahin Sonmez and Saffet Ayasun, 'Stability Delay Margin Computation of Load Frequency Control System with Demand Response,' 1st IEEE Global Power Energy and Communication Conference (GPECOM 2019), June 12-15, 2019, Cappadocia, Turkey.

9) H. Bevrani, A. Ghosh, and G. Ledwich, "Renewable energy sources and frequency regulation: survey and new perspectives," *IET Renew·able Power Generation*, vol. 4, no. 5, pp. 438-457, Sept. 2010.

10) W. Kempton and S. Letendre, "Electric vehicles as a new power source for electric utilities," *Transportation Research Part D*, vol. 2, no. 3, pp.157-175, Sept.

1997.

11)   J. R. Pillai and B. Bak-Jensen, "Integration of vehicle-to-grid in the western Danish power system," *IEEE Transactions on Sustainable Energy*, vol. 2, no. 1, pp. 12-19, Jan. 2011.

12)   M. Y. Mu, J. Wu, J. Ekanayake *et al.*, "Primary frequency response from electric vehicles in the Great Britain power system," *IEEE Trans·actions on Smart Grid*, vol. 4, no. 2, pp. 1142-1150, Jun. 2013.

13)   C. Guille and G. Gross, "A conceptual framework for the vehicle-to- grid (V2G) implementation," *Energy Policy*, vol. 37, no. 11, pp. 4379- 4390, Nov. 2009.

14)   S. Han, S. Han, and K. Sezaki, "Development of an optimal vehicle- to-grid aggregator for frequency regulation," *IEEE Transactions on Smart Grid*, vol. 1, no. 1, pp. 65-72, Jun. 2010.

15)   R. J. Bessa and M. A. Matos, "The role of an aggregator agent for EV in the electrical market," in *Proceedings of 7th Mediterranean Confer·ence and Exhibition on Power Generation, Transmission, Distribution and Energy Conversion*, Agia Napa, Cyprus, Nov. 2010, pp. 7-10.

16)   R. J. Bessa, M. A. Matos, and F. J. Soares, "Framework for the partici·pation of EV aggregators in the electricity market," in *Proceedings of 2014 IEEE International Electric Vehicle Conference (IEVC)*, Flor·ence, Italy, Dec. 2014, pp. 1-8.

17)   A. M. Carreiroa, H. M. Jorge, and C. H. Antunesa, "Energy manage·ment systems aggregators: a literature survey," *Renewable and Sustain·able Energy Reviews*, vol. 73, pp. 1160-1172, Jun. 2017.

18)   C. Quinn, D. Zimmerle, and T. H. Bradley, "The effect of communica·tion architecture on the availability, reliability, and economics of plug- in hybrid electric vehicle-to-grid ancillary services," *Journal of Power Sources*, vol. 195, no. 5, pp. 1500-1509, Mar. 2010.

19)   K. Ko and D. K. Sung, "The Effect of cellular network-based communication delays in an EV aggregator' s domain on frequency regulation service," *IEEE Transactions on Smart Grid*, vol. 10, no. 1, pp. 65-73, Jan. 2019.

20)   K. Mak and B. L. Holland, "Migrating electrical power network SCA·DA systems to TCP/IP and ethernet networking," *Power Engineering Journal*, vol. 16, no. 6, pp. 305-311, Dec. 2002.

21)   K. S. Ko and D. K. Sung, "The effect of EV aggregators with time- varying delays on the stability of a load frequency control system,"computation of quasi-polynomial zeros," *IEEE Transactions on Auto·matic Control*, vol. 54, no. 1, pp. 171-177, Jan. 2009.

22)   K. S. Ko, S. Han, and D. K. Sung, "A new mileage payment for EV aggregators with varying delays in frequency regulation service," *IEEE*

Transactions on Smart Grid, vol. 9, no. 4, pp. 2616-2624, Jul. 2018.

23)   H. Fan, L. Jiang, C. K. Zhang *et al*., "Frequency regulation of multi- area power systems with plug-in electric vehicles considering communication delays," *IET Generation, Transmission & Distribution*, vol. 10, no. 14, pp. 3481-3491, Nov. 2016.

24)   R. Sipahi and I. I. Delice, "Advanced clustering with frequency sweeping methodology for the stability analysis of multiple time-delay sys·tems," *IEEE Transactions on Automatic Control*, vol. 56, no. 2, pp. 467-472, Feb. 2011.

25)   I. Delice and R. Sipahi, "Delay-independent stability test for sys·tems with multiple time-delays," *IEEE Transactions on Automatic Control*, vol. 57, no. 4, pp. 963-972, Apr. 2012.